Random tilings with quasicrystal order: transfer-matrix approach

1988 J. Phys. A: Math. Gen. 21 1649

(http://iopscience.iop.org/0305-4470/21/7/028)

J. Phys. A: Math. Gen. **21** (1988) 1649-1677. Printed in the UK

Random tilings with quasicrystal order: transfer-matrix approach

Christopher L Henley†
Department of Physics, Cornell University, Ithaca, NY 14853-2501, USA

Received 15 July 1987

Abstract. The random tiling of the plane by a set of objects (e.g., rhombi), related by rotational (e.g., tenfold) symmetries, is a paradigm for the formation of quasiperiodic order due to entropy. Such tilings are mapped to a higher-dimensional space where they form hypersurfaces analogous to the interfaces in a solid-on-solid model. I argue that the fluctuations of the hypersurface should be described by a gradient-squared free energy of entropic origin; this implies quasi-long-range order in $d = 2$. I show how the random tiling can be decomposed into layers, define a transfer matrix, and give prescriptions for using this method to determine numerically the stiffness of the gradient free energy.

1. Introduction

The distinguishing characteristic of experimental quasicrystals is that they have non-crystallographic fivefold symmetries but rather sharp diffraction peaks (Shechtman *et al* 1984). It was natural to model their structures by ideal deterministic quasicrystals. These are packings or tilings of identical rigid units, which are perfectly quasiperiodic, i.e. their diffraction patterns consist entirely of Bragg peaks of zero width (Levine and Steinhardt 1984, Elser 1985b, Katz and Duneau 1986).

However, it is now generally accepted that all the real rapidly quenched alloys incorporate a large amount of structural disorder (Heiney *et al* 1987). The observed high resistivity and diffuse scattering might be explained by merely local (e.g., substitutional) disorder, but the observed broadening of the diffraction peaks indicates some kind of disorder in the long-range geometry. Furthermore, there are great difficulties even in formulating ideal model systems of interacting atoms with deterministic quasicrystal ground states‡. There is still controversy over the nature, and degree, of this disorder (Elser 1985a, b, 1987, 1988, Stephens and Goldman 1986, Lubensky *et al* 1986, Horn *et al* 1986) and whether it is intrinsic to quasicrystal formation (Elser 1985a, 1987, Stephens and Goldman 1986, Henley 1987).

Random tilings are the simplest random quasicrystal models. In this paper, two ways of representing random tilings are used. One way, which has proved both physical

† Present address: Department of Physics, Boston University, Boston, MA 02215, USA.

‡ Such structures have the disconcerting property that atoms must jump suddenly in response to small changes of their surroundings (Frenkel *et al* 1986). This suggests that metastability and disorder occur in practice.

0305-4470/88/071649+29$02.50

and practical in other contexts, is to lift them into hypersurfaces in a space of D dimensions. Then, well understood concepts from interface theory can be carried over to model the statistical physics of this hypersurface. It turns out that the long-range correlations depend on the fluctuations of the hypersurface normal to the physical space.

Elser (1987) has conjectured that a simple gradient-squared free energy (equation (2.12)) gives the statistical weight of these fluctuations. This gives a simple basically entropic mechanism whereby long-range quasicrystal order develops in $d > 2$ (Elser 1985b, 1988). It is desirable to test the correctness of this picture and numerically calculate its parameters: the stiffness K of the gradient-squared free energy and the entropy S_0 of the random tiling. These parameters are important for models of real systems, which are described by geometries similar to a random tiling. The stiffness K affects the diffraction pattern (Elser 1985b) and the residual entropy S_0 affects the thermodynamic stability of the quasicrystal phase.

The second way to represent the tilings is to decompose them into rows, where each row is a string of sites and each site has a finite set of states as in a spin model. This is the necessary basis of transfer-matrix schemes, which are the focus of this paper.

1.1. Models of disorder in quasicrystals

The structure of quasicrystals has most fruitfully been described by a 'rigid geometry plus decoration' approach. Such a structural model consists of (i) the geometry—rigid framework or network, built by repeated use of identical, and identically oriented, geometrical units—and (ii) the decoration—a rule for placing atoms on the rigid geometry. My only concern in this paper is the geometry, which is responsible for any possible long-range quasicrystal order. The most popular geometries are as follows.

(i) Networks of icosahedra, connected by bonds along symmetry directions (Shechtman *et al* 1984, Stephens and Goldman 1986, Guyot and Audier 1985, Elser 1988, Henley 1988). The two-dimensional analogues are networks of decagons (or pentagons).

(ii) Tilings of rhombohedra (Elser and Henley 1985, Henley and Elser 1986) or other polyhedra (Henley 1988); the two-dimensional analogues being rhombi or other polygons, such as triangles and squares.

I define '(translational) long-range order' to mean 'existence of Bragg scattering'. The Penrose tiling (de Bruijn 1981) and its generalisations to other symmetries (Socolar *et al* 1985) are geometries analogous to perfect crystal lattices. Their Fourier transform consists of nothing but Bragg peaks—they have *perfect*, albeit non-periodic, long-range order—and they have no residual entropy: $S_0 = 0$ (Gähler 1986). More realistic models must incorporate microscopic disorder, $S_0 > 0$, but not every kind of disorder will destroy the long-range correlations.

A possible picture of the quasicrystal state is that the geometry is such a perfect arrangement, but with defects called 'phasons' superimposed (Socolar *et al* 1986). Most models, however, use geometries with built-in randomness, and are intended to show that disorder is somehow *intrinsic* to the formation of quasicrystals (Elser 1987, Stephens and Goldman 1986). One major category of random models is the *growth models*, in which icosahedra or decagons are aggregated in a non-equilibrium growth process which mimics the rapid quenching needed to produce most quasicrystals (Stephens and Goldman 1986, Elser 1987, 1988, Minchau *et al* 1987).

Another major category of random models is *equilibrium* models which possess a partition function, and thus have some hopes of analytic treatment. For example,

simulations have been performed of objects interacting in two dimensions: two-component systems of particles with radially symmetric interactions (Widom *et al* 1987, Lançon *et al* 1986, Leung *et al* 1988) and also decagon systems with angularly dependent interactions (Elser 1987). The potentials are chosen so that the ground state is a rigid geometry with a non-zero ground-state entropy S_0, implying disorder (Widom *et al* 1987, Leung *et al* 1988).

The simplest models are tiling models. Like the Penrose tilings (and generalisations that have been devised), they consist of a few classes of identical tiles, packed edge-to-edge without gaps or overlaps, and with no other restrictions on which edges may adjoin. (In contrast, in ideal Penrose tilings (de Bruijn 1981), rhombus edges are labelled with arrows to enforce 'matching rules' and this restriction suffices to reduce the entropy to zero.) The degrees of freedom are discrete but infinite in number. We could formulate a growth model with tiles rather than decagons (Elser 1985a). However, in this paper I will consider only *equilibrium* models of random tilings. They may be a Hamiltonian assigning different energies to different kinds of vertex, or, most simply, we can weight all distinct packings equally ('equal-weighted ensemble'), an equilibrium model with an entirely entropic 'free energy.'

1.2. Previous estimates of parameters for two-dimensional geometries

Several estimates have been made of the entropy S_0 of random quasicrystal tilings and networks. Here I discuss the methods and compare the numerical values. Note that I define S_0 as entropy per unit area; I will measure the area in units of $\bar{A}$, which is defined as the average area per tile, in tilings which have a statistical p-fold symmetry in the orientations of different kinds of rhombi (i.e. zero phason strain, see § 2.3). When the tiling in question actually has this symmetry, the entropy in these units is just the entropy per unit rhombus (note also the number of rhombi must equal the number of vertices). The most plausible values for the tenfold tiling are all consistent with $S_0 \approx 0.5\bar{A}^{-1}$.

(i) For tilings made by a random growth process, one can record the number of choices available for each new site that is added. An average of the logarithm of this quantity gives a crude estimate of the entropy per site. For a tenfold random tiling (with the number rato of fat to thin tiles constrained to have the same number ratio τ as occurs for tenfold symmetry), Chen and Spaepen (1987) found $S_0 \sim 0.495\bar{A}^{-1}$. Of course, the entropy in the growth-process ensemble is not the same as that of the maximum-entropy ensemble.

(ii) For a random tiling, one gets a simple estimate from counting the number of configurations available in a finite region. For example, in the 2D tenfold rhombus tiling, a decagon can be packed in 62 possible ways with ten rhombi (these are shown in Frenkel *et al* (1986), figure 11). Here $A = (5+2\sqrt{5})\bar{A} \simeq 9.47\bar{A}$, giving $S_0 \approx \ln(62)/A \simeq 0.436\bar{A}^{-1}$.

(iii) Chen and Spaepen (1988) have taken a kind of statistical mean-field approach to the entropy, in the spirit of Pauling's approximate entropy for the ice model as used by Spaepen (1976). They consider the many different types of vertex possible in the tiling, and consider each vertex to be chosen at random where the corners of the two kinds of tiles are weighted with activities so as to ensure the overall number ratio of large rhombi to small rhombi is $\tau \equiv (\sqrt{5}+1)/2$. They find $S_0 \simeq 0.64$ per rhombus. We would expect this to be an overestimate, since the constraints between the local environments of neighbouring vertices are neglected.

(iv) The approach in this paper was inspired by the use of transfer matrices to generate random square-triangle tilings and evaluate their entropy S_0 (Kawamura 1983).

Kawamura found a one-to-one mapping of triangle-square tilings to packings of triangles and 60° rhombi; this can be treated as a triangular lattice with rules for erasing some edges (more complicated than the analogous rules for the tiling in figure 1(*b*)). Each vertex was considered as having one of eight different states, corresponding to its local environment in the tiling. A necessary and sufficient condition for a configuration to represent a square-triangle tiling is to satisfy a four-spin constraint around every rhombic plaquette generated by the two basis vectors. (The constraint is that the plaquette must be in one of 107 states, out of the 8^4 possible states.) These transfer matrices are very sparse and break up into disconnected blocks. The approach I consider in this paper describes the possible states more transparently.

The triangle-square tilings have 12-fold symmetry and so, according to the arguments of § 2 (below), they should be random quasicrystals. However, Kawamura considered these tilings as models of an amorphous state and did not investigate correlation functions which might have revealed translational order.

(v) A Monte Carlo approach has been used by Orrick (1987). The method is as follows: for the case of a 2D rhombus tiling (Elser 1985a) one can generate new tilings by a sequence of 'reshuffling' moves, each of which moves only one vertex and the neighbouring three rhombi†. It appears that this is ergodic, i.e. one can get from any tiling (of a finite region) to any other one by such moves. Thus, doing this flip on randomly chosen vertices gives a Monte Carlo dynamics which should generate the correct random-tiling ensemble, if we are in equilibrium. Let us impose a Hamiltonian for which the ground state is a perfect Penrose tiling, which has zero entropy; the infinite-temperature state is the equal-weighted random-tiling ensemble. Thus, the entropy of the latter state is the integral $\int_0^\infty \mathrm{d}T(C(T)/T)$ where $C(T)$ is the specific heat, measured through the Monte Carlo. Orrick (1987) used an artificial 'potential', $V=\frac{1}{2}|\boldsymbol{h}^\perp|^2$, where $\boldsymbol{h}^\perp$ is the perpendicular fluctuation mentioned above and discussed extensively in § 2.

For a random tiling with eightfold symmetry, Orrick (1987) finds an entropy of $S_0 \simeq 0.3943$ per rhombus, using square systems of 41, 239 and 1393 rhombi (these choices minimised the phason strain by using rational approximants to $\sqrt{2}$). Note that the value for sixfold symmetry is 0.3383 per rhombus (see § 3.2) so that, as we would expect, the entropy for p-fold symmetric tilings grows monotonically with p. It is interesting to note that rapidly quenched VNiSi and CrNiSi alloys have been reported to be described by a random tiling with eightfold symmetry (Wang *et al* 1987).

Thus, many methods exist to estimate the entropy S_0. On the other hand, the only previously suggested approach for determining the stiffness K is the Monte Carlo method just described (Elser private communication). One need only measure (at $T=\infty$) the equilibrium fluctuations $\langle|\boldsymbol{h}^\perp(\boldsymbol{r})-\boldsymbol{h}_0^\perp|^2\rangle$, where $\boldsymbol{h}_0^\perp$ is the average through the sample, and this gives K by finite-size scaling (in the spirit of § 5.2 below). Such an approach has one advantage over the transfer-matrix method proposed in this

† This Monte Carlo procedure is far simpler than that for the simulations of interacting particles (Widom *et al* 1987, Leung *et al* 1988) since (a) the state space is discrete rather than continuous, and (b) for the simplest case, the Boltzmann weights are all equal. For the 3D rhombohedral tiling, there is an analogous move of one vertex corresponding to a repacking of four rhombohedra. However, such moves do not appear to exist for the 2D square-triangle tiling (Leung *et al* 1988) or the 3D icosahedrally symmetric 'canonical cell' tiling (Henley 1988).

paper: one can study (toy model) dynamics. At large length scales, the Monte Carlo dynamics should have diffuse phasons (Bak 1985, Lubensky *et al* 1985, Socolar *et al* 1986), which do not seem to exist in non-random models (Frenkel *et al* 1986).

Unfortunately, the fluctuations of $\boldsymbol{h}^{\perp}$ were not measured in the simulation of Orrick (1987). However, Elser (1987) did measure them in simulations of a growth model.

1.3. Outline of the paper

The purpose of this paper is to present a method to determine S_0 and K numerically, in the two-dimensional case, by transfer matrices. In the rest of the paper, I first (§ 2) introduce the D-dimensional formalism with the concepts of phason strain, the coarse-grained free energy and the correlation functions. Next (§ 3) I discuss (as a pedagogical example) a random tiling which has sixfold symmetry and thus is *not* a quasicrystal. First it is shown how this corresponds to an interface in a $D=3$ cubic lattice. Then an efficient prescription is given for representing configurations of the tiling by dividing them into rows, and transition rules are given which define the transfer matrix. Section 4, the core of the paper, repeats this work for the case of the randomised Penrose tiling with tenfold quasicrystal symmetry. Then § 5 develops the ideas introduced in § 2 to work out the relation of the transfer matrices to the macroscopic free energy and correlation functions, so that the parameters of the free energy can be extracted from transfer-matrix iteration using finite-size scaling. Section 6 concludes with a discussion of possible elaborations, modifications or applications of this method. An appendix gives, as an example, calculations of the entropy for very small strips, of width up to four.

2. Approaches to random quasicrystals

2.1. D-dimensional representation

It is elegant, convenient and useful to represent the rigid geometries discussed in § 1.1 by embedding them in a periodic lattice in a higher dimension D. A given vertex of the geometry with coordinates $\boldsymbol{r}^{\parallel}$ in the d-dimensional 'physical' space can be written

$$\boldsymbol{r}^{\parallel} = \sum_{\alpha=1}^{D} x_\alpha \hat{\boldsymbol{e}}^{\parallel}_{(\alpha)} \tag{2.1a}$$

in terms of unit basis vectors $\hat{\boldsymbol{e}}^{\parallel}_{(\alpha)}$ (with integer-valued $[x_\alpha]$). We define the $d^{\perp}$-dimensional 'complementary' coordinate

$$\boldsymbol{h}^{\perp} = \sum_{\alpha=1}^{D} x_\alpha \boldsymbol{e}^{\perp}_{(\alpha)}. \tag{2.1b}$$

The basis vectors are chosen so that in D-dimensional space,

$$\boldsymbol{e}_{(\alpha)} \equiv (d^{\parallel}/D)^{1/2} \hat{\boldsymbol{e}}^{\parallel}_{(\alpha)} + \boldsymbol{e}^{\perp}_{(\alpha)} \tag{2.2}$$

form an orthonormal set†. The specifics of this 'lifting' are left to §§ 3.1 and 4.1 which give detailed examples.

† The choice to normalise physical and perpendicular space in different ways is the source of various factors of $d^{\parallel}/D$ in subsequent formulae.

I will use $d^{\parallel}$ as a synonym of d when I wish to emphasise the dual roles of physical and perpendicular space. For the sixfold tiling considered in § 3, $(d^{\parallel}, d^{\perp}, D) = (2, 1, 3)$; for the tenfold tiling considered in § 4, $(d^{\parallel}, d^{\perp}, D) = (2, 3, 5)$; and for icosahedral symmetry, $(d^{\parallel}, d^{\perp}, D) = (3, 3, 6)$. For quasicrystals, which have non-crystallographic symmetries by definition, we always have $d^{\perp} \geqslant 2$.

Then in D-space the vertex is a lattice vector with coordinates $[x_\alpha]$ of the hypercubic lattice generated by $\boldsymbol{e}_{(\alpha)}$. The sum $\boldsymbol{r}^{\parallel} + \boldsymbol{h}^{\perp}$ describes the same vertex but in coordinates rotated so as to break up the physical and complementary subspaces. In fact, equations (2.1) give this rotation; its inverse is

$$x_\alpha = (d^{\parallel}/D)\hat{\boldsymbol{e}}^{\parallel}_{(\alpha)} \cdot \boldsymbol{r}^{\parallel} + \boldsymbol{e}^{\perp}_{(\alpha)} \cdot \boldsymbol{h}^{\perp}. \tag{2.3}$$

Neighbouring objects, if connected by a bond of the proper orientations and length, lift up into neighbouring lattice sites in D dimensions; thus, a connected geometry lifts to a network in D-space. It can be shown that Bragg diffraction—i.e. long-range order—exists if and only if this network is localised in the $\boldsymbol{h}^{\perp}$ direction (Elser 1985b). In turn, we would expect that the spread of $\boldsymbol{h}^{\perp}$ depends on how constrained the geometry is. Quasicrystal geometries fall along a sort of spectrum according to how random and how well connected the network is. Closely related to this is their behaviour in D-space. For a perfect quasicrystal, the embedded network approximates $\boldsymbol{h}^{\perp} =$ constant as closely as possible. This defines a *hypersurface* in D-dimensional space.

The opposite extreme of disorder occurs when nearby objects are not necessarily connected by a bond of proper orientation and length, e.g., in the so-called 'icosahedral glass' model (Stephens and Goldman 1986). The bond network can be broken by extended wall defects; they correspond in D-space to breaks or 'tears' in the fabric of the hypersurface (Elser 1987, 1988), across which $\boldsymbol{h}^{\perp}$ changes discontinuously. This is believed to spread out $\boldsymbol{h}^{\perp}$ and destroy the Bragg scattering.

The random-tiling models studied in this paper belong to an intermediate class where the network, although non-deterministic, is well connected. It defines a continuous map from d-space into D-space, with a rippled but unbroken hypersurface. (Such fluctuations are called 'phasons'.) Such structures can even be produced in growth models, if the growth rates and thermal gradients are chosen properly (Elser 1987, 1988).

Ideas borrowed from the interface physics will be used throughout this paper to understand the hypersurface $\boldsymbol{h}^{\perp}(\boldsymbol{r}^{\parallel})$. A 'solid-on-solid' restriction is customary in interface physics whereby overhangs are forbidden by fiat; here it arises naturally since the tiles do not overlap in $\boldsymbol{r}^{\parallel}$-space. Then $\boldsymbol{h}^{\perp}(\boldsymbol{r}^{\parallel})$ is the analogue of the interface height. Whether the distribution of $\boldsymbol{h}^{\perp}$ is localised or not is analogous with whether an interface is localised or rough†.

Do geometries of the intermediate class have long-range order? One can easily construct geometries of this type where the long-wavelength deviation of the ripples from $\boldsymbol{h}^{\perp} =$ constant is unbounded and destroys Bragg diffraction. However, the known properties of roughening behaviour of the interfaces strongly suggests that the constraints that the network be connected are powerful enough to suppress such large fluctuations, preserving Bragg peaks (though with reduced intensities (Elser 1985b) and diffuse wings, analogous to effects of lattice vibrations in ordinary crystals). Such

† This connection should not be confused with recent work on real interfaces of quasicrystals in physical space (Henley and Lipowsky 1987, Garg and Levine 1987, Ho *et al* 1987). Also, the D-dimensional embedding here is distinct from that in 'crumpling' models (Kantor *et al* 1986) which lack the solid-on-solid constraint.

random geometries with non-crystallographic symmetry that still possess Bragg peaks will be called *random quasicrystals.*

2.2. Phason strain

The tilings made by the 'cut-and-project' method (Elser 1985b, Katz and Duneau 1986) approximate a plane $\boldsymbol{h}^{\perp} = \text{constant}$, i.e. parallel to the plane of the physical subspace. As we have defined the physical hyperplane, its orientation in the 6D lattice has special high *symmetry* but is also *incommensurate* (i.e. the hyperplane does not contain any direction with all indices rational in terms of the 6D basis). More generally, we can consider a hyperplane

$$\boldsymbol{h}^{\perp} \simeq \mathbf{E}\boldsymbol{r}^{\parallel} + \text{constant} \tag{2.4}$$

where $\mathbf{E}$ is the $d^{\perp} \times d^{\parallel}$ tensor called the 'phason strain' (Socolar *et al* 1986, Lubensky *et al* 1986); this defines the orientation. Another parametrisation of this hypersurface is $x_{\alpha} = \boldsymbol{m}_{(\alpha)} \cdot \boldsymbol{r}^{\parallel} + \text{constant}$ where

$$\boldsymbol{m}_{(\alpha)} \equiv \nabla_{\parallel} x_{\alpha} = (d/D)\hat{\boldsymbol{e}}^{\parallel}_{(\alpha)} + (\boldsymbol{e}^{\perp}_{(\alpha)} \cdot \mathbf{E}) \tag{2.5}$$

the last equality following from (2.3).

Depending on whether the orientation is commensurate or incommensurate, the resulting structure may be either a crystal (Elser and Henley 1985, Katz and Duneau 1986) or else an incommensurately modulated quasicrystal.

We can define a uniform phason strain even for structures that are not described by a flat hypersurface like (2.4), by taking the limit as $|\boldsymbol{r}| \to \infty$ of the ratio of components $\boldsymbol{h}^{\perp}$ to $\boldsymbol{r}^{\parallel}$. This is defined if the fluctuations $\boldsymbol{h}^{\perp}(\boldsymbol{r}^{\parallel}) - \boldsymbol{h}^{\perp}(\mathbf{0})$ grow more slowly than $|\boldsymbol{r}^{\parallel}|$, which is true for $d \geqslant 1$ (see (2.18)); I will call a hyperplane with this orientation an 'approximating plane.'

2.3. Rhombus frequencies

Consider the case of tilings in $d^{\parallel} = 2$ with p-fold symmetry. We can label each type of rhombus (distinguishing orientations) by α, β where the edges in the physical tiling are $\hat{\boldsymbol{e}}^{\parallel}_{(\alpha)}$ and $\hat{\boldsymbol{e}}^{\parallel}_{(\beta)}$, and we choose $(\hat{\boldsymbol{e}}^{\parallel}_{(\alpha)} \times \hat{\boldsymbol{e}}^{\parallel}_{(\beta)}) > 0$ to make the labelling unique. (I use the scalar-valued 2D cross product with $(1, 0) \times (0, 1) = 1$.) Also, let the number density (per unit area) of these rhombi be $n_{\alpha\beta}$ and let $n_{\beta\alpha} = -n_{\alpha\beta}$. Each such rhombus corresponds to a square in the hypercubic lattice plane spanned by $\hat{\boldsymbol{e}}_{(\alpha)}$, $\hat{\boldsymbol{e}}_{(\beta)}$. Consequently, $n_{\alpha\beta}$ is equal to the direction cosine relating this plane to the approximating plane, that is

$$\begin{aligned} n_{\alpha\beta} &= \boldsymbol{m}_{(\alpha)} \times \boldsymbol{m}_{(\beta)} \\ &= (d/D)\hat{\boldsymbol{e}}^{\parallel}_{(\alpha)} \times \hat{\boldsymbol{e}}^{\parallel}_{(\beta)} + c_{\alpha\beta,mi} E_{mi} + \boldsymbol{e}^{\perp}_{(\alpha)} \times \boldsymbol{e}^{\perp}_{(\beta)} \det(\mathbf{E}). \end{aligned} \tag{2.6}$$

The constant term is just d/D times the area of the rhombus,

$$A_{\alpha\beta} \equiv \hat{\boldsymbol{e}}^{\parallel}_{(\alpha)} \times \hat{\boldsymbol{e}}^{\parallel}_{(\beta)}.$$

This shows how the number density is very generally proportional to the area of the rhombus (provided we maintain true p-fold symmetry, i.e. $\mathbf{E} = \mathbf{0}$).

The coefficients of the linear term are defined by

$$c_{\alpha\beta,mi} E_{mi} \equiv (d/D)[(\hat{\boldsymbol{e}}^{\perp}_{(\alpha)} \cdot \mathbf{E}) \times \hat{\boldsymbol{e}}^{\parallel}_{(\beta)} - (\boldsymbol{e}^{\perp}_{(\alpha)} \cdot \mathbf{E}) \times \boldsymbol{e}^{\parallel}_{(\beta)}]. \tag{2.7}$$

For small phason strains, we can linearise (2.6), $\delta n_{\alpha\beta} = c_{\alpha\beta,mi} E_{mi}$.

Since the $e^{\perp}$ are chosen to satisfy (2.2), it turns out that the coefficient in the third quadratic term in (2.6), $e^{\perp}_{(\alpha)} \times e^{\perp}_{(\beta)}$, is the same for all rhombi types related by a simple rotation. Hence, the imbalance of rhombus types which is entailed by $\mathbf{E} \neq \mathbf{0}$ is all in the linear term.

We can think of $c_{\alpha\beta,mi}$ as being a tensor with $D(D-1)/2 \times d^{\perp} d^{\parallel}$ non-trivial components, e.g., 10×6 for the Penrose tiling. (There are $D(D-1)/2$ different kinds of rhombi, counting different orientations.) The existence of an approximating plane puts constraints on the possible sets of $\{n_{\alpha\beta}\}$, since $c_{\alpha\beta,mi}$ has rank less than $D(D-1)/2$. There must be at least $D(D-1)/2 - d^{\perp} d^{\parallel} = d^{\perp}(d^{\perp}-1)/2 + d^{\parallel}(d^{\parallel}-1)/2$, constraints (e.g. four for the tenfold rhombus tiling).

What are the null and non-null spaces of $c_{\alpha\beta,mi}$ for the tenfold projection? It is helpful to think in terms of the cyclic group generated by permutation (12345) applied to α and β (which is a rotation by $2\pi k/5$) and the representations of this group. Then we find that $c_{\alpha\beta,mi}$ for $m = 1, 2$ couples only to 'angular momentum' $m = \pm 1$ and $c_{\alpha\beta,3i}$ couples only to 'angular momentum' $m = \pm 2$.

'Angular momentum' zero corresponds to two constraints. One is trivial: the total area density $\frac{1}{2}\Sigma A_{\alpha\beta} n_{\alpha\beta}$ must be unity. Since $A_{\alpha\beta}$ is invariant under rotations, $\Sigma_{\alpha\beta} A_{\alpha\beta} c_{\alpha\beta,mi} \equiv 0$ identically. For the non-trivial constraint let $\varepsilon_{\alpha\beta} = \mathrm{sgn}(A_{\alpha\beta})$ so that

$$\bar{n}_{\mathrm{tile}} \equiv \tfrac{1}{2} \sum_{\alpha\beta} \varepsilon_{\alpha\beta} n_{\alpha\beta} \tag{2.8}$$

is the total number of rhombi per unit area. Again, since $\varepsilon_{\alpha\beta}$ is symmetric under rotations one finds $\Sigma_{\alpha\beta} \varepsilon_{\alpha\beta} c_{\alpha\beta,mi} \equiv 0$ identically:

$$\delta \bar{n}_{\mathrm{tile}} = 0 \tag{2.9}$$

to $\mathrm{O}(\mathbf{E})$. In fact, $\delta \bar{n}_{\mathrm{tile}} / \bar{n}_{\mathrm{tile}} = 1 - (D/d^{\parallel}) \tau^{-3} \det(\mathbf{E})$.

2.4. Coarse-graining: free energy and correlation functions

Consider now the random tiling model with all configurations weighted equally, and coarse-grain the $\boldsymbol{r}^{\parallel}$ coordinate so that $\boldsymbol{h}^{\perp}(\boldsymbol{r}^{\parallel})$ becomes continuous-valued and slowly varying. Within the scale of the coarse graining, we can define an approximating plane with phason strain

$$\mathbf{E} \equiv \nabla_{\parallel} \boldsymbol{h}^{\perp}. \tag{2.10}$$

Different configurations of our new coarse-grained $\boldsymbol{h}^{\perp}$ are no longer equally weighted: in integrating out the short-wavelength fluctuations we pick up a free energy

$$\tilde{F} = \int \mathrm{d}^{d} \boldsymbol{r}^{\parallel} \, \sigma(\mathbf{E}). \tag{2.11}$$

Here $\sigma(\mathbf{E})$ is the analogue of the surface energy as a function of surface orientation in an interface model (see, e.g., Rottman and Wortis 1984).

The basis vectors are always chosen with high symmetry in both physical and complementary spaces. It follows that the orientation of the physical plane given by $\mathbf{E} = \mathbf{0}$ has a unique high symmetry in the hypercubic lattice† (e.g., in figure 1(*b*) this is the ⟨111⟩ orientation). By symmetry, then, $\mathbf{E} = \mathbf{0}$ must be a stationary point of $\sigma(\mathbf{E})$

† Yet, in the quasicrystal case, this special orientation is also incommensurate. This combination of special symmetry and incommensurateness is foreign to our intuition, since it can occur only in lattices of dimension $D \geq 4$.

as a function of $\mathbf{E}$. Furthermore, as shown in § 2.3, this is the only possible $\mathbf{E}$ that corresponds to a tiling which has, for each type of rhombus, equal numbers in all possible orientations related by symmetry. This makes it plausible that $\mathbf{E}=\mathbf{0}$ is a *maximum* of the entropy, i.e. a minimum of $\sigma(\mathbf{E})$.

Interestingly, Kawamura (1983) found that the maximum entropy in a triangle-square tiling occurs when $n_\triangle/n_\square \approx 0.45$. By a slight adaptation of (2.6), one finds that ideally $n_\triangle/n_\square = \sqrt{3}/4 \simeq 0.433$ in the tiling with 12-fold symmetry; hence Kawamura's result supports the conjecture that $\mathbf{E}=\mathbf{0}$ is the maximum of the entropy.

Finally, assuming $\sigma(\mathbf{E})$ is analytic we get

$$\sigma(\mathbf{E}) = \tfrac{1}{2}K(\mathbf{E})^2 = \tfrac{1}{2}K(\nabla_\parallel \boldsymbol{h}^\perp)^2 \tag{2.12}$$

as the lowest power allowed by symmetry. Provided the symmetry operations mix different components of the physical and complementary subspaces, all of the $d^\parallel d^\perp$ terms in (2.12) have the same coefficient $\frac{1}{2}K$, where K is called the 'phason stiffness'. (An example where the complementary space is reducible into unmixed and inequivalent subspaces, with different stiffnesses, is found in (4.2).)

2.5. Free energy with phason strain

We could imagine introducing a Hamiltonian (with temperature divided out) of the form

$$\tilde{H} = \tfrac{1}{2}\sum_{\alpha,\beta} f_{\alpha\beta} n_{\alpha\beta}. \tag{2.13}$$

This is to be added to the integrand in (2.11).

The $f_{\alpha\beta} = -f_{\beta\alpha}$ are chemical potentials for the different tiles and orientations exactly as introduced in dimer models (Kasteleyn 1963). For small $f_{\alpha\beta}$, this should be a weak perturbation of the random tiling.

Substituting (2.13) into (2.7) to linearise in $\mathbf{E}$ gives

$$\delta\tilde{H} = \tfrac{1}{2}\sum_{\alpha\beta} f_{\alpha\beta}\delta n_{\alpha\beta} = \tfrac{1}{2}\sum_{m=1}^{d^-}\sum_{i=1}^{d^\parallel} F_{mi}E_{mi} \tag{2.14}$$

where

$$F_{mi} \equiv \sum_{\alpha\beta} c_{\alpha\beta,mi} f_{\alpha,\beta}. \tag{2.15}$$

The total free energy will now have the form

$$\tilde{F} = \tilde{H}(\mathbf{E}) - \sigma(\mathbf{E}). \tag{2.16}$$

The first term is the coupling (2.13) (linearised in (2.14)), and the second term is the entropy, the quadratic gradient-squared term in (2.12). Thus, we expect in general a linear response $\mathbf{E} = K^{-1}\mathbf{F}$ of the phason strain to imposed chemical potentials such as (2.13).

A particularly interesting case is if we choose

$$f_{\alpha\beta} = P\varepsilon_{\alpha\beta}$$

in (2.13), thus coupling to the total number of rhombi $\bar{n}_{\text{tile}}$. Since the total area is fixed in our ensemble, $P>0$ favours thin rhombi, and hence P can be identified with the *pressure*. But from (2.9), $\mathbf{F}=\mathbf{0}$ in this case, and there is no linear response: $\mathrm{d}^2S/\mathrm{d}P^2 = 0$. In other words, the random tiling with p-fold symmetry is incompressible.

Obviously the map in (2.15) of possible $\{f_{\alpha,\beta}\}$ onto $\mathbf{F}$ is many-to-one. But provided that $c_{\alpha\beta,mi}$ has full rank (this is true for the sixfold or tenfold tilings), the map in (2.15) is onto, so that we can favour any desired phason strain by some choice of chemical potentials $f_{\alpha\beta}$. As we vary chemical potentials, interesting phase transitions are expected (Kawamura 1983, Blöte and Hilhorst 1982). In this paper, however, only the response to small chemical potentials is considered.

2.6. *Correlation function*

In general we can define an interface correlation function by

$$G(\boldsymbol{r}^{\parallel}) \equiv \langle |\boldsymbol{h}^{\perp}(\boldsymbol{r}^{\parallel}) - \boldsymbol{h}^{\perp}(\boldsymbol{0}) - \mathbf{E}_0 \boldsymbol{r}^{\parallel}|^2 \rangle. \tag{2.17}$$

We can now derive (2.17) from the free energy (2.12) in a standard fashion, since the integral is Gaussian and trivial in Fourier space. (The case $d = 2$ is done in more detail in § 5.)

The result is

$$\begin{aligned} G(\boldsymbol{r}^{\parallel}) &\sim |\boldsymbol{r}^{\parallel}|^{2-d} && d < 2 \\ &\sim \ln|\boldsymbol{r}^{\parallel}| && d = 2 \\ &\sim \text{constant} && d > 2. \end{aligned} \tag{2.18}$$

(Note how, since the free energy (2.12) is quadratic, the form of the correlation function depends only on the dimension $d^{\parallel}$ of the *physical* space.) The behaviour in $d^{\parallel} = 2$ dimensions is marginal. For $d^{\parallel} = 2$, there will be algebraic singularities indicating quasi-long-range order, as occurs even in two-dimensional crystals at $T > 0$ due to phonons. Power-law cusps replace Bragg peaks in the diffraction pattern.

It is amusing to consider the shape of a peak. Its centre is at $\boldsymbol{Q}^{\parallel}$, a Bragg peak of the perfect quasicrystal, and hence (Elser 1985b) a projection of a D-dimensional reciprocal lattice vector $\boldsymbol{Q} = \boldsymbol{Q}^{\parallel} + \boldsymbol{Q}^{\perp}$. We can use $\boldsymbol{Q}^{\parallel} \cdot \boldsymbol{r}^{\parallel} + \boldsymbol{Q}^{\perp} \cdot \boldsymbol{h}^{\perp} = 0 \pmod{2\pi}$ (before coarse graining) to rewrite the intensity near the peak as

$$I(\boldsymbol{Q}^{\parallel} + \delta\boldsymbol{q}^{\parallel}) \sim \int \mathrm{d}^2\boldsymbol{r}^{\parallel} |\boldsymbol{r}^{\parallel}|^{-\eta} \exp(\mathrm{i}\delta\boldsymbol{q}^{\parallel} \cdot \boldsymbol{r}^{\parallel}) \tag{2.19}$$

where

$$\eta = \tfrac{1}{2} C |\boldsymbol{Q}^{\perp}|^2 \tag{2.20}$$

and C is the prefactor of the logarithm in (2.18). Since the reciprocal lattice contains arbitrarily small $\boldsymbol{Q}^{\perp}$ vectors, it follows that peaks exist which are arbitrarily close in shape to being Bragg peaks.

It is conceivable that the argument of § 2.4 breaks down, i.e. that $\mathbf{E} = \mathbf{0}$ is not a minimum, that $\sigma(\mathbf{E})$ is non-analytic there, or that $K = 0$. Then the fluctuations, and the critical dimension for order, would be different than (2.18). A central motivation for this paper, then, is to develop a means of testing whether the quadratic form (2.12) is correct.

3. Sixfold rhombus tiling

As a simple example to motivate and clarify the Penrose tiling discussion, let us consider arbitrary tilings of the plane by rhombi with unit length edges and acute angle

60° (Elser 1984), as in figure 1. We wish to study the statistical properties of the equal-weighted random-tiling ensemble (every possible distinct tiling has equal probability). In this section, I only show how to represent such tilings and the rules for constructing strips of the equal-weighted random tiling by a transfer matrix.

Before beginning, let us note that (i) the possible tilings have sixfold rotational symmetry, which is crystallographic, and (ii) the *vertices* always form a perfect periodic triangular lattice. Thus, these tilings are *not* quasicrystals in any sense.

(*a*) *Exact solution.* In fact, the sixfold random-tiling model corresponds (Elser 1984, Blöte and Hilhorst 1982) to solved models. Note that the dual of the triangular lattice is a honeycomb lattice. Each rhombus covers two adjacent honeycomb sites. Thus, the tiling configurations corresponds one-to-one to ways of laying dimers on a honeycomb lattice so as to cover all of its sites once.

The random-dimer model, with equal weight to each allowed configuration, was solved exactly by Kasteleyn (1963) for the dimer representation; his solution also permits different activities for dimers in different orientations.

There is also a one-to-one correspondence (Blöte and Hilhorst 1982) between tiling configurations and the ground states of the antiferromagnetic Ising model on a triangular lattice (Wannier 1950): the broken lines in figure 1 correspond to the frustrated bonds.

3.1. Representation by lift to a three-dimensional lattice

Following Elser (1984) we can assign $D = 3$ dimensional coordinates to each vertex as follows. Pick one vertex to be the origin $\mathbf{0}$. Obviously any vertex $\boldsymbol{r}$ can be represented in the form (2.1*a*) $\boldsymbol{r}^{\parallel} = \sum_{\alpha=1}^{3} x_\alpha \hat{\boldsymbol{e}}_\alpha^{\parallel}$, with integer coefficients x_α. The basis vectors $\hat{\boldsymbol{e}}_\alpha^{\parallel}$ are manifestly dependent over integers so this does not suffice to define the $[x_\alpha]$.

The prescription to define the $[x_\alpha]$ uniquely is to draw a path from $\mathbf{0}$ to $\boldsymbol{r}$ along the tile edges, and then let x_α be the number of times this path goes in each of the three possible directions $\hat{\boldsymbol{e}}_\alpha^{\parallel}$ counting negatively when it goes in the opposite sense. Now if the counts from two paths differ, this difference is the sum along the loop made up by the two paths. But this sum, in turn, is equal to a sum over loops around each rhombus contained within the larger loop, and obviously the sum around each

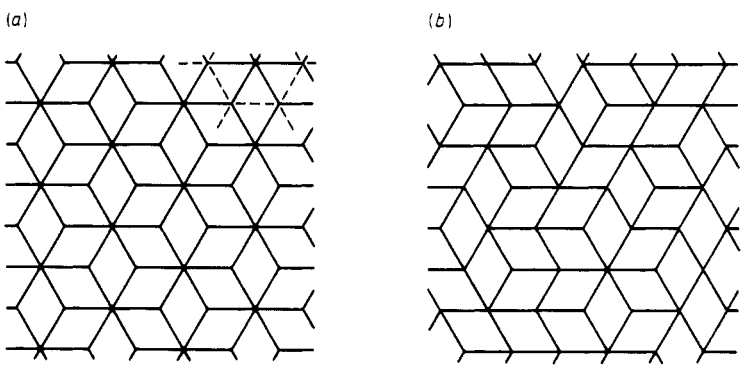

Figure 1. Tilings by 60° rhombi. The vertices form a triangular lattice; every bond of the lattice is either a tile edge or a tile bisector (some of these are shown as broken lines). (*a*) Periodic tiling; this is the projection of the ⟨111⟩ interface of a simple cubic lattice. (*b*) Random tiling.

rhombus is zero: this shows the uniqueness. (This argument obviously works for *any* tiling composed only of rhombi.)

We can consider the $[x_\alpha]$ as being coordinates in a 3D simple cubic lattice. The 3D basis vectors are given by (2.2) with

$$\boldsymbol{e}_i^\perp = (a/\sqrt{3})\hat{z} \tag{3.1}$$

for $i = 1, 2, 3$, with $\hat{z}$ being a unit vector normal to the plane of $\boldsymbol{r}^\parallel$. As is obvious from a glance at figure 1, the rhombus tiling is a projection of an interface composed of the square faces of cells of the cubic lattice. The periodic tiling in figure 1(a) approximates a plane $\boldsymbol{h}^\perp$ = constant as closely as possible. The set of all tilings corresponds one-to-one with the set of interfaces which (when viewed at this orientation) have no overhangs.

Note that the diffraction pattern of such a tiling depends on the fluctuations of $\boldsymbol{h}^\perp$ if and only if the decoration depends on which edges are broken in figure 1.

3.2. Layer representation and transition rules

For a transfer-matrix calculation, we describe the system as a strip with width W. The system must be decomposed into one-dimensional layers of width W, and its degrees of freedom must be divided among them. Each configuration of the system is described by a well defined sequence of layer states, each of which is a string of steps each of which can take values from a discrete list.

If necessary (not the case here, but it is the case for the tenfold tiling, § 4) there should be rules describing which sequences of steps are forbidden either because (a) they are impossible in an infinite tiling, or (b) they are equivalent to some other sequence, and we require a one-to-one description. This ensures that there are no 'dead ends', i.e. every layer state has at least one possibility for the next one.

Furthermore, we require necessary and sufficient conditions to determine which patterns of layer states correspond to tilings, and which are impossible. These have the form of 'transition rules' which tell which layer states can follow which layer states. Given these rules, it must also be checked that the map from tilings to sequences of layers is one-to-one.

3.2.1. Decomposition rules. It is natural to choose the strip to run in a symmetry direction. There are two kinds of symmetry directions—six running along edges, $\hat{\boldsymbol{e}}_i^\parallel$, and six normal to edges; the transition rules are much simpler if we use one of the latter directions. Then each layer is a line of triangular lattice bonds. As illustrated in figure 2, we write a layer state as a sequence of symbols 1 (representing a bond which is present as a tile edge) and 0 (representing a bond which is absent since it bisects a rhombus). The sequence for the next layer is considered to be offset by a half-space. We assume periodic boundary conditions throughout.

3.2.2. Transition rules. Given one layer, which states are possible for the next one? Consider the edges which connect the two layers. Above each 0 bond, we must have a $-\hat{e}_3^\parallel$ edge, tilting to the right, and an $\hat{e}_2^\parallel$ edge, tilting to the left, joining to meet above. Above any other segment, the vertical edges from the right end and the left end must tilt in the same way, since it makes a rhombus. This already confirms part of the one-to-one condition: from each allowed pattern of 1- and 0-bonds, at most one tiling can be reconstructed (we need no additional degrees of freedom to describe the vertical bonds).

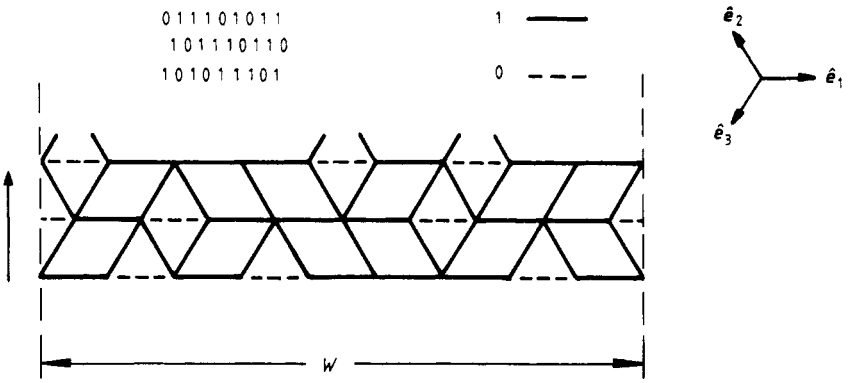

Figure 2. Transfer matrix implementation for a strip of width $W = 9$. The strip is grown upwards (arrow). The 'horizontal' segments making up a layer are indicated by full lines. The same configuration is represented above by a binary code. The inset shows the numbering convention for the basis vectors $\hat{\boldsymbol{e}}_i^{\parallel}$.

Let us define an 'interval' of length l to be a sequence of $l-1$ 1-bonds bounded by a 0 on the left and on the right; in the new row, this corresponds to an interval of length l between the vertices above the 0-bonds. By the above observation, the new row must have (i) l_L 1-bonds, corresponding to tiles with $\hat{\boldsymbol{e}}_2$ edges (tilting left); (ii) one 0-bond corresponding to a single vertex in the old row with both an $\hat{\boldsymbol{e}}_2^{\parallel}$ edges and an $-\hat{\boldsymbol{e}}_3^{\parallel}$ edge coming out upwards, and (iii) l_R 1-bonds, where $l = l_L + l_R + 1$, corresponding to tiles with $\hat{\boldsymbol{e}}_3^{\parallel}$ edges (tilting right).

Our rule for sequences can now be stated: within each interval, exactly one 0-bond must appear in the new layer, and it can be anywhere in this interval (l possibilities). Also, it is easy to see that any sequence of layers following this rule can be reconstructed into a tiling, which confirms the rest of the one-to-one condition. Note that the number of 0-bonds is the same in each row.

The enumeration of states of the next layer is very simple. Let us describe a layer by writing the lengths $\{l_i\}$ of the intervals of starting with each 0 and continuing up to the next 0. Note $\Sigma_i l_i = W$. Thus, $011101001 \rightarrow 4, 2, 1, 2$ (for $W = 9$, periodic boundary conditions). For the ith interval, there is one 0 in the next layer at one of l_i possible positions. Note that the choice in one interval is completely independent of the choice in the next. The total number of possible configurations of the new layer is thus

$$\prod l_i. \tag{3.2}$$

3.2.3. Estimate of entropy of steps within layers. We can derive a rigorous (and close) upper bound on the true entropy using (3.2). By the Gershgorin theorem (see, e.g., Wilkinson 1965), given a matrix $\mathbf{T}$ with non-negative entries, its maximum eigenvalue satisfies $\Lambda_0 \leqslant \Sigma_\beta T_{\beta\alpha}$ for any α. But the RHS of this inequality is just (3.2); it is maximised by setting all l_i to the value l that maximises $\ln l/l$, namely $l_i \equiv 3$. Note this is just a layer from the ideal tiling of figure 1(a), so that the deviation of $\boldsymbol{h}^{\perp}$ within the layer averages to zero. This makes it plausible that the maximum-entropy orientation of the approximating plane is close to $\mathbf{E} = \mathbf{0}$ as discussed in § 2.4.

The corresponding entropy is

$$S_0 \leqslant S_{\text{est}} = \tfrac{1}{3} \ln 3 \approx 0.3662. \tag{3.3}$$

There is exactly one step per tile, so (3.3) is also an estimate of the entropy per tile. The exact transfer-matrix calculation for width $W=3$ reduces to a 1×1 matrix with value 2, which gives the same value (3.2) as the exact entropy for this width. For comparison, the exact value for the unbounded lattice (Wannier 1950) is $S_0 \simeq 0.3383$.

3.3. Correlations between steps in a layer

What is the typical layer state in the random tiling? One might guess that it is just a random sequence of 0- and 1-bands. But if this were right, the correlation function $G(\boldsymbol{r}^{\parallel})$ would grow as $|\boldsymbol{r}^{\parallel}|^{1/2}$, along this string. This would contradict the result (2.18), derived from the 'free energy' (2.12), which gives only a logarithmic growth. The resolution is that the dominant layer states in the random tiling are *not* random sequences; they are those sequences that lead to many possibilities for the next layers, and this constraint is enough to change the typical fluctuations. The correct weighting must incorporate long-range correlations between steps in the layers which suppress fluctuations of $\boldsymbol{h}^{\perp}$.

A plausibility argument to exhibit how this happens in the language of layers is as follows. The long-range correlations arise from the step-conserving nature of the transition rule. Consider a fluctuation of $h^{\perp}$ with wavelength W' in one layer: the weight $\Pi\, l_i$ will be reduced by a factor $\exp[-c(\delta h^{\perp})^2/W']$, as in the weighting of a 1D random walk, for *every* layer in which this is true. We estimate the typical fluctuation $\boldsymbol{h}^{\perp}$ for a given W' as that value which makes the argument of the exponential be of order unity. If we only took the above weight, corresponding to a fluctuation in just one layer, we would obtain the incorrect $(W')^{1/2}$ behaviour. However, the number of iterations required to remove the fluctuation is at least $O(W')$ so the effect of the fluctuation on the weight of the whole tiling is exponentiated $O(W')$ times, which cancels the $1/W'$ in the argument of the exponential. This crude balancing argument is too crude to see the logarithm and would now suggest the expected deviation $\delta h^{\perp}$ grows at worst as W'^{0}. Including the sum of all the shorter-wavelength fluctuations should give a logarithmic behaviour in the transverse direction, in agreement with (2.18) (and with (5.14)).

4. Random tenfold tiling

In this section, I turn to tilings made with the Penrose rhombi. These have acute angles 72° and 36° for the large and small rhombus, respectively, making possible a tenfold orientational symmetry. There are five different edge vectors $\hat{\boldsymbol{e}}_i^{\parallel}$. Regular and random tilings with these rhombi are shown in figure 3. (The golden ratio $\tau \equiv 2\cos(2\pi/5) \equiv (1+\sqrt{5})/2$ appears frequently in the formulae below.)

Tilings can be analysed in the same two ways presented in § 3. However, there are some additional conceptual and technical problems to sort out. (This should not be surprising, as there are 54 possible vertex types in this tiling compared with five types for the sixfold tiling.)

4.1. Representation in five-dimensional space

The tilings correspond one-to-one to faceted hypersurfaces in a $D=5$ dimensional hypercubic lattice, where now $d^{\perp}=3$. We have $\boldsymbol{r}^{\parallel}$ and $\boldsymbol{h}^{\perp}$ given by (2.1). The 5D coordinate $[x_\alpha]$ is well defined by the uniqueness argument of § 3.1.

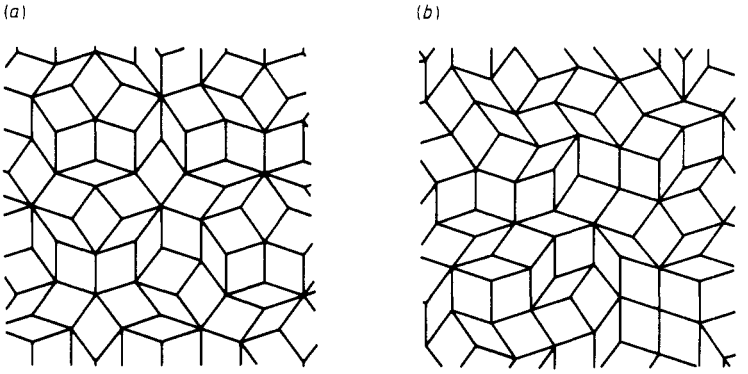

Figure 3. (*a*) Deterministic Penrose tiling of 36° and 72° rhombi. (*b*) Random tiling of the same rhombi.

The basis vectors $\hat{\boldsymbol{e}}^{\parallel}_{(\alpha)}$ are shown in figure 4, and in complementary space

$$\boldsymbol{e}^{\perp}_{(1,2,3,4,5)} \equiv (\sqrt{\tfrac{2}{5}}\,\hat{\boldsymbol{e}}^{\parallel}_{(1,3,5,2,4)},\ \sqrt{\tfrac{1}{5}}). \tag{4.1}$$

There is a technical complication of the embedding in 5-space. The third component of $\boldsymbol{h}^{\perp}$ is aligned along the $\langle 11111\rangle$ axis in 5-space: in this one direction, the complementary subspace is oriented *commensurately*. Thus, the third component is always a multiple of $\sqrt{\frac{1}{5}}$. It is exactly analogous to the one component of $\boldsymbol{h}^{\perp}$ in § 3.

The consequence is that there is no symmetry relating the third component to the other two. Equation (2.12) will now contain two stiffnesses:

$$\delta S = -\int \mathrm{d}^2\boldsymbol{r}^{\parallel}[\tfrac{1}{2}K(|\nabla h_1^{\perp}|^2+|\nabla h_2^{\perp}|^2)+\tfrac{1}{2}K_3|\nabla h_3^{\perp}|^2]. \tag{4.2}$$

Since the third component is commensurate, deterministic tilings made by the cut-and-project technique with $\boldsymbol{h}^{\perp} \simeq \boldsymbol{h}^{\perp}_{(0)}$ have different distributions of local environments, depending on the value of $h_3^{\perp}\ (\mathrm{mod}(\sqrt{\frac{2}{5}}))$. We might expect this to carry over into the coarse-grained free energy for *intermediate* length scales as a periodic potential term, $V(h_3^{\perp})$. If $V(\cdot)$ is stronger than a critical value, then it becomes infinitely strong at large length scales and $h_3^{\perp}$ is localised. When $V(\cdot)$ becomes weaker than this critical amount, there is a roughening transition and it becomes zero at the longest length scale. Presumably the random-tiling model corresponds to the second case. However, if energy terms are added that implement the 'matching rules' or otherwise favour the vertices of a particular $h_3^{\perp}$, then we might see the localised-$h_3^{\perp}$ phase at low temperatures.

The tenfold-symmetric networks of Elser (1987) contain pentagons: since the sum of $\boldsymbol{e}_{\alpha}$ vectors around a pentagon is non-zero, the above embedding scheme fails. Instead, he uses a less obvious embedding scheme which evades the technical complication. In terms of the same basis vectors $\{\hat{\boldsymbol{e}}^{\parallel}_{\alpha}\}$ and $\{\boldsymbol{e}^{\perp}_{\alpha}\}$ edges are represented by $(1,-1,0,0,0),\ldots$, rather than $(1,0,0,0,0),\ldots$. Then $h_3^{\perp} \equiv 0$, while $\boldsymbol{r}^{\parallel}$ and the first two components of $\boldsymbol{h}^{\perp}$ are merely dilated and rotated.

4.2. Representation in layers

In contrast to the sixfold tiling (§ 3), here it is not altogether obvious how the tiling should be organised into layers. We consider a strip with its longitudinal (here, vertical) axis oriented along one of the tile-edge directions. Figure 4 shows how we may draw

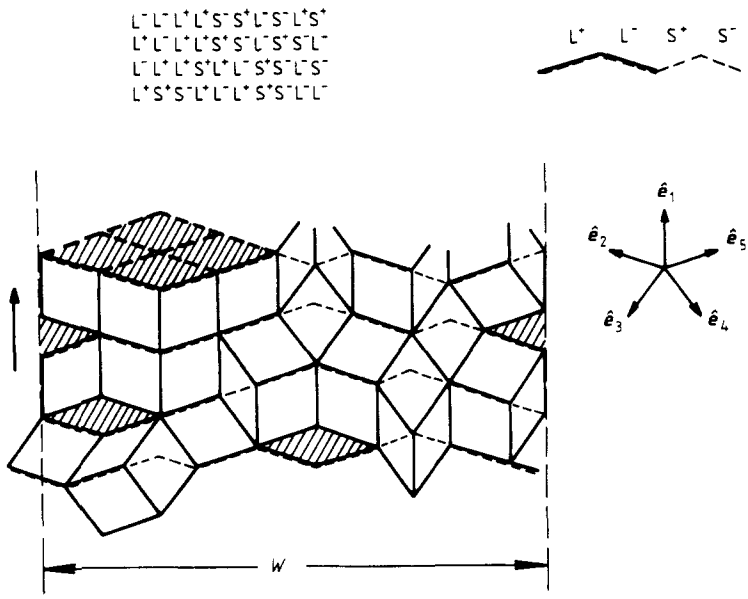

Figure 4. Implementation of the transfer matrix for the tiling of 36° and 72° rhombi. The segments making up a layer are indicated by full lines. The same configuration is represented above by strings of $L^{\pm}$, $S^{\pm}$. Intermediate layers of horizontal thin rhombi are hatched; the possibilities for the next layer are indicated by broken lines. The inset shows the numbering convention for the basis vectors $\hat{e}_i^{\parallel}$.

layers across the tiling from left to right, each consisting of a string of 'steps'. The rules are as follows.

Decomposition rule (*i*). Every edge in the direction $\hat{e}_5^{\parallel}$ or $-\hat{e}_2^{\parallel}$ becomes a long step L^+ or L^-, except for those covered in rule (iv).

Decomposition rule (*ii*). In each thin rhombus with one edge vertical (i.e. along $e_1^{\parallel}$), the short diagonal becomes a short step $S^{\pm}$. Note S^+ (S^-) is in the same direction as L^+ (L^-) but is shorter by a factor τ.

Decomposition rule (*iii*). Every fat rhombus with its long axis vertical is a special case: we span its short axis by S^+S^-. This means that we do not distinguish it, at this point, from a pair of thin rhombi. Indeed, these can always fit in the 72° angle of the fat rhombus. However, we can always distinguish these possibilities by the sequence in the *next* layer: the pair of thin rhombi forces another 72° angle, and hence another S^+S^-, in the next layer, while the fat rhombus never does so.

Decomposition rule (*iv*). Thin rhombi with their long axis horizontal are a special case, since both their top and bottom edges are made of $\hat{e}_5^{\parallel}$ and $\hat{e}_2^{\parallel}$ vectors which are normally $L^{\pm}$. For each such rhombus (or domain of contiguous rhombi of this kind), only the *lowermost* edges become $L^{\pm}$.

Observe that the rhombi which require special cases are those which are symmetric about the vertical axis. Rules (iii) and (iv) are basically arbitrary choices—we could have chosen S^-S^+ in rule (iii), or chosen the uppermost edge in (iv), as is very obvious if we imagine how to represent the same tiling reflected about the horizontal axis.

It can easily be checked that, by these rules (especially rule (iv)), each vertex has exactly one step entering from the left and one step leaving to the right, except for some vertices which by rule (iv) have no steps on either side. Thus, each distinct layer is well defined. As will be shown shortly in § 4.3, the number of steps across the strip,

N_W, is the same for every layer (assuming periodic boundary conditions). Every string of $L^{\pm}$, $S^{\pm}$ corresponds to a possible layer. Each layer has $N_\mu = 4^{N_W}$ possible configurations.

For a given phason strain $\mathbf{E}$, we can deduce the numbers of $L^{\pm}$ and $S^{\pm}$ in each layer and the conversion factors N_W/W (steps per unit width) and N_L/L (number of layers per unit distance vertically, i.e. longitudinally). We let $n(L^+)$, $n(L^-)$, $n(S^+)$ and $n(S^-)$ be the respective number densities of the different kinds of steps per unit area of the tiling. Counting the contribution of each rhombus type,

$$\begin{aligned} n(L^+) &= (n_{45}+n_{51})+n_{35} \\ n(L^-) &= (n_{23}+n_{12})+n_{24} \\ n(S^+) &= n_{34}+n_{41} \\ n(S^-) &= n_{34}+n_{13}. \end{aligned} \tag{4.3}$$

(In each equation, the left-hand term corresponds to fat tiles and the right one to thin ones.) All tile types are counted once in (4.3) except horizontal thin rhombi (n_{52}) and vertical fat rhombi (n_{34}) because of the special rules (iii) and (iv), so

$$\bar{n}_{\text{step}} \equiv n(L^+)+n(L^-)+n(S^+)+n(S^-) = \bar{n}_{\text{tile}}+n_{34}-n_{52} \tag{4.4}$$

($\bar{n}_{\text{tile}}$ is given by (2.8)). The number densities $n_{\alpha\beta}$ can in turn be calculated from (2.6).

Now, for the tenfold symmetric case, $\mathbf{E}=\mathbf{0}$, the number fractions of fat and thin tiles are τ^{-1} and τ^{-2}, so

$$n(L^+) = n(L^-) = [2(\tau^{-1}/5)+(\tau^{-2}/5)]\bar{A}^{-1} = (\tau/5)\bar{A}^{-1} \tag{4.5a}$$

$$n(S^+) = n(S^-) = [(\tau^{-1}/5)+(\tau^{-2}/5)]\bar{A}^{-1} = (1/5)\bar{A}^{-1} \tag{4.5b}$$

where

$$\bar{A} \equiv (\tau^{-1}+\tau^{-3})\sin(2\pi/5)$$

is the average area per tile. Thus the total density of steps is

$$(N_W/W)(N_L/L) = \bar{n}_{\text{step}} = (2/5)\tau^2\bar{A}^{-1} \simeq 0.9960. \tag{4.6}$$

From equations (4.5) we see that, within each layer, the number ratio of $L^{\pm}$ to $S^{\pm}$ must be τ; the average width per step turns out to be the same number, $\bar{A}$. With (4.5), this finally gives

$$(W/N_W) = \bar{A} \simeq 0.95\ldots \tag{4.7}$$

$$(L/N_L) = 2\tau^2/5 \simeq 1.0472. \tag{4.8}$$

4.3. Transition rule for new layer

With the arbitrary choice used in decomposition rule (iv) the iteration should start from layers that take the *lowermost* edges of domains of horizontal thin rhombi; however, the most important transition rule starts from a layer along the *uppermost* edges. Therefore, let us first imagine what can go between this layer with uppermost edges and the next layer with lowermost edges. The relatively trivial transition rule LL (below), which takes us from a layer with lowermost-edges chosen layer to one with uppermost edges chosen, will be described last although it comes first in the iteration.

From each vertex of the old layer, bonds can extend near-vertically in any of three directions, $-\hat{\boldsymbol{e}}_4^{\parallel}$, $\hat{\boldsymbol{e}}_1^{\parallel}$ or $-\hat{\boldsymbol{e}}_3^{\parallel}$. Now note that, so long as we add rhombi, we must use

the *same* kind of 'vertical' bond over each vertex, and so the sequence in the next layer is exactly the same. The only possible changes are associated with *triangles*, i.e. bisected rhombi, appearing between the layers. In § 3, these were associated with 0 steps; here they are associated with $S^{\pm}$ steps. As before, we can divide each layer into *intervals* between $S^{\pm}$ from which we see transition rule LS.

Transition rule LS.

(a) In any interval bounded by (S^-, S^+), the next layer has *no* $S^{\pm}$.

(b) In any interval bounded by $(S^-, S^-]$, the next layer has *one* S^-; similarly, in any interval bounded by $[S^+, S^+)$, the next layer has *one* S^+.

(c) In any interval bounded by $[S^+, S^+]$, the next layer has one S^+, and then one S^-.

(d) The $L^{\pm}$ sequence in the new layer is not changed by this rule.

Obviously, the number of steps of each type is conserved from layer to layer. Transition rule LS can be simplified as follows: an S^+ (S^-) always moves zero or more places to the right (left) by exchanging places with $L^{\pm}$, up to, but not over, the next $S^{\pm}$.

The special cases in decomposition rules (iii) and (iv) are reflected in special transition rules SS and LL.

Transition rule SS. A vertical fat rhombus is represented by S^+S^-, but in the next layer it looks like it had been S^-S^+. So, following decomposition rule (iii) above, we need a special rule which says that it is possible (but not required) to switch $S^+S^- \rightarrow S^-S^+$ before applying rule LS. (If we only had rule LS, all the $S^{\pm}$ steps would eventually pile up in immobile S^+S^- pairs.)

Transition rule LL. The canonical layer defined by the decomposition rules of § 4.2 followed the lowermost edges of domains of thin horizontal rhombi, but transition rules LS and SS start from layers which follow the uppermost edges. Therefore, these rules must actually be prefaced by a rule that describes all possible intervening domains of horizontal thin rhombi. The upper edges are a path across the grid defined by $\boldsymbol{e}_5^{\parallel}$, $-\boldsymbol{e}_2^{\parallel}$. Hence, the rule states that a path is allowed if and only if it always stays above the path of the lower edges.

Transition rule LL can be reworded as: within each interval, we can have any permutation of the $L^{\pm}$ that can be made by moving L^+ (L^-) steps to the left (right) by exchanges.

4.4. Counting possibilities for transfer matrix.

Although the total number of new configurations is $O(e^W))$, it is possible to compute how many there are and to select one at random in a time of $O(W)$ because different lanes do not interact in the transition rules. This is very advantageous for the Monte Carlo transfer-matrix method (see § 5.3) and is also convenient for estimates analogous to equation (3.3).

The rules are applied in the order LL, SS and LS. Rule LL does not change the interval structure; thus, for a given starting layer state, the set of possibilities is the direct product of the $L^+ \leftrightarrow L^-$ permutations of rule LL and the $S^+ \leftrightarrow S^-$ moves of rules LS and SS.

For rule LL, there is a simple algorithm to compute the number of possible arrangements of the upper path over the thin rhombi, and also to select one of these at random with equal weights. Figure 5 shows the set of all possible paths. Place a weight 1 on the leftmost node; then moving to the right, place on each node a weight $\omega_1 + \omega_2$ where ω_1, ω_2 are the weights of the left neighbours: the final weight is the number of possible paths. To select a path at random, follow a path from right to

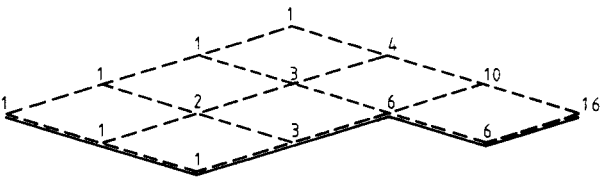

Figure 5. Counting possible ways to add thin rhombi, starting with an interval with six $L^{\pm}$ steps, $L^-L^-L^+L^+L^-L^+$.

left; at each node with two left neighbours, step to neighbour i with probability $\omega_i/(\omega_1+\omega_2)$. The maximum possible number for rule LL occurs for the lowest lower surface, corresponding to $L^-L^- \ldots L^+L^+$. If the number of $L^{+,-}$ is m_+, m_-, the possible new paths are any permutation of $L^{\pm}$ which gives $(m_+ + m_-)!/m_+!\, m_-!$ possibilities.

For rule LS, given an interval of l steps†: for case (a) there is only one possibility in the next layer; for case (b), there are l choices for places to put one $S^{\pm}$ within the interval and it is easy to choose one at random; for case (c) there are $l(l-1)/2$ choices and it is still easy to choose one at random.

The only difficulty in enumerating the choices is the effect of rule SS. In that case, when a single pair is permuted $S^+S^- \rightarrow S^-S^+$, the intervals on both sides come under case (b) instead of (a), or case (c) instead of (b), in rule LS, i.e. these intervals do interact. Let us group the intervals into strings, such that intervals separated by S^+S^- pairs are tied into the same string. Fortunately, not all $S^{\pm}$ are in pairs, so the strings are finite and different strings do not interact.

To deal with such a string, note that each S^+S^- pair has two degrees of freedom, like an Ising spin. It is possible to count the possible states of the string by multiplying a string of symmetric (2×2) transfer matrices $\Pi\, \mathbf{M}_i$, where

$$\mathbf{M}_i \equiv \begin{pmatrix} l_i(l_i-1)/2 & l_i \\ l_i & 1 \end{pmatrix}$$

for each interval of length l_i between two pairs. As with rule LL, we can select a state by following the iteration in reverse.

As in the derivation of (3.3), we could in principle find an upper bound for the entropy of the random tenfold tiling; however, in this case it is far from trivial to determine $\max_\alpha(\Sigma_\alpha T_{\beta\alpha})$.

5. Extracting parameters from the transfer-matrix calculation

In this section, I consider how one could analyse transfer-matrix results so as to determine the parameters S_0 and K. In fact, S_0 is the logarithm of the dominant eigenvalue and how to obtain it is obvious; therefore, I focus on K. Several independent measurable quantities are exhibited from which K can be found, which should provide a useful check on the results, and I discuss which of these quantities are easier to compute with transfer matrices.

For discussions of finite-size scaling in related systems, see Luck (1982).

† In defining the length of an interval, every S^+ (S^-) is counted with the interval to its right (left).

5.1. Transfer-matrix formulation

To set up a transfer matrix, we must first choose a strip width and a composition of step types. For the tenfold tiling, from equations (4.5), the only composition corresponding to zero phason strain and tenfold symmetry is $n(L^+) = n(L^-) = n_L$, $n(S^+) = n(S^-) = n_S$ and $n_L/n_S = \tau$, which is manifestly impossible for finite N_W. The best we can do is to choose n_L/n_S to be one of the rational approximants to τ, F_{k+1}/F_k, where F_k is the kth Fibonacci number. (In fact (see equation (5.13) and § 5.6), the simplest method to determine K demands that we iterate the transfer matrix with various phason strains, i.e. various compositions of steps.) Note that $n(L^+) \neq n(L^-)$ or $n(S^+) \neq n(S^-)$ implies that a layer is not exactly normal to the symmetry direction.

The N_W steps now give a space of $N_\mu = k_{\text{step}}^{N_W}$ layer states (where k_{step} is the number of step types). The transfer matrix $\mathbf{T}$ then has $T_{\nu\mu} = 1$ if the transition rules allow successive layers $\mu \to \nu$ (with chemical potentials (2.13) included, this is replaced by a weight); otherwise $T_{\nu\mu} = 0$.

The transition rules LS, SS and LL of § 4.3 define partial transfer matrices which I will call $\mathbf{T}_{LS}$, $\mathbf{T}_{SS}$ and $\mathbf{T}_{LL}$, respectively, so I have

$$\mathbf{T} = \mathbf{T}_{LS}\mathbf{T}_{SS}\mathbf{T}_{LL}. \tag{5.1}$$

Note that $\mathbf{T}$ is *not* generally a symmetric matrix by the definition (5.1).

I have formulated the transfer matrix to add an entire layer at a time. For spin models, it has been found useful to impose spiral boundary conditions which allows adding only one site at a time in the transfer matrix, so that it is very sparse. This also seems feasible for tilings, by an adjustment of the boundary conditions—it would correspond to a strip with a long axis that deviates slightly from the symmetry direction. However, this is probably less important in this system where all new layer states have equal, or comparable, statistical weights, or else do not occur at all, and where every state leads to many new states.

5.1.1. Symmetries of the transfer matrix. For a strip with balanced numbers of each type of step, $n(L^+) = n(L^-)$, $n(S^+) = n(S^-)$, we also have reflections about the longitudinal (x) direction as well as the transverse (y) direction, since we iterate along a symmetric direction of the tiling. However, for a general strip we only have a twofold rotation (with axis normal to the plane of the strip). This can be implemented by a permutation matrix π, i.e. $\mathbf{T} \to \pi\mathbf{T}\pi$. In the layer representation, this corresponds to rewriting the string of $L^\pm$ and $S^\pm$ backwards for each layer, and furthermore to reversing the sequence of layers.

We have:

$$\mathbf{T}_{LL}^{\mathrm{T}} = \pi\mathbf{T}_{LL}\pi \qquad \mathbf{T}_{LS}^{\mathrm{T}} = \pi\mathbf{T}_{LS}\pi \qquad \mathbf{T}_{SS}^{\mathrm{T}} = \pi\mathbf{T}_{SS}\pi. \tag{5.2}$$

Thus, $\mathbf{T}^{\mathrm{T}} = \pi\mathbf{T}_{LL}\mathbf{T}_{SS}\mathbf{T}_{LS}\pi$. Also, from § 4.3 it is clear that $\mathbf{T}_{LL}$ and $\mathbf{T}_{SS}$ commute, so we can write

$$\mathbf{T}^{\mathrm{T}} = \mathbf{M}\mathbf{T}\mathbf{M}^{-1} \tag{5.3}$$

with $\mathbf{M} = \pi\mathbf{T}_{LL}\mathbf{T}_{SS}$. (Any generic real matrix is similar to its transpose, but here the similarity represents a symmetry.)

The rules of § 4.3 have an additional amusing symmetry which is not a tiling symmetry: $\mathbf{T}_{LL}$ is invariant under replacing every S^+ by S^- and vice versa in every string, while $\mathbf{T}_{LS}$ and $\mathbf{T}_{SS}$ are similarly invariant under $L^+ \leftrightarrow L^-$.

5.1.2. Eigenvalues of transfer matrices. As is usual with transfer matrices, the highest eigenvalue Λ_0 is real and gives the entropy $S_0 \propto \ln \Lambda_0$. The next-highest eigenvalue Λ_1 describes the decay of order—if there is long-range order it has the same magnitude $|\Lambda_1| = \Lambda_0$ in the $W \to \infty$ limit, but there is a gap for finite W. A new feature here is that Λ_1 is complex, $\Lambda_1 = |\Lambda_1| e^{i\theta_1}$ as different kinds of layers tend to succeed each other in a quasiperiodic cycle.

We can find the fundamental 'frequency' θ_1 by considering the decomposition of the regular Penrose tiling into layers. Some layers straddle rows of tiles with $\hat{\boldsymbol{e}}_1^{\parallel}$ edges that are dual to grid lines (de Bruijn 1981) running in the layer direction. These layers are separated by narrow or wide 'lanes' (Henley and Lipowsky 1987) with respectively one or two intervening layers. The lanes form a Fibonacci sequence so that the average spacing between similar layers† is τ^2 layers, i.e. $\theta_1 = 2\pi/\tau^2$.

In fact θ_1 is proportional to the projection $\hat{\boldsymbol{e}}_1^{\parallel} \cdot \boldsymbol{g}_{(1)}^{\parallel}$ where $\boldsymbol{g}_{(1)}^{\parallel}$ is the (10000) reciprocal lattice basis vector, i.e. its projection on the longitudinal strip direction. In the ideal tiling $\boldsymbol{g}_{(1)}^{\parallel} \equiv \frac{2}{5}(2\pi)\hat{\boldsymbol{e}}_{(1)}^{\parallel}$. In the presence of phason strain, $\boldsymbol{g}_{(1)}^{\parallel} \to \boldsymbol{g}_{(1)}^{\parallel} - \mathbf{E}^{\mathrm{T}} \boldsymbol{g}_{(1)}^{\perp}$ where $\boldsymbol{g}_{(\alpha)}^{\perp} \equiv (2\pi)\boldsymbol{e}_{(\alpha)}^{\perp}$ are the complementary-space basis vectors in the ideal tiling. Choosing coordinates so that the strip axis $\hat{\boldsymbol{e}}_{(1)}^{\parallel}$, and $\boldsymbol{e}_{(1)}^{\perp}$, are all along $(1, 0)$, we obtain

$$\theta_1 = (2\pi)\tau^{-2}(1 - \sqrt{\tfrac{5}{2}}E_{11} - \sqrt{\tfrac{5}{4}}E_{31}). \tag{5.4}$$

There is a subtle difficulty: the transfer-matrix procedure describes a fixed-N_{L} ensemble, not the desired fixed-L ensemble, where L is the length. Maximising the entropy per layer is not equivalent to maximising the entropy per unit area, because some layers are thicker than others and tend to have more entropy per step. A bias to thicker layers, i.e. smaller $\bar{n}_{\mathrm{step}}$ (see § 4.2) will induce a phason strain as if a chemical potential of form (2.13) had been added, coupling to $\bar{n}_{\mathrm{step}}$ (which by (4.4) and (2.9) means coupling to $n_{34} - n_{52}$). To obtain the desired result, we must add a compensating chemical potential by hand, calculating the entropy for different values and finding the maximum (i.e. we must do a Legendre transform).

5.2. Correlation functions and finite-size scaling

We will work out the finite-size scaling properties (dependence on the width W) of the correlation function $G(\cdot)$ defined in (2.17), limiting ourselves to $d^{\parallel} = 2$ dimensions. We write W as a superscript on the correlation functions to remind us that they depend on the width. The reader may wish to refer to finite-size scaling analysis by Luck (1982) for the XY model.

5.2.1. Bulk correlation function. Let us first find $G(\boldsymbol{r}^{\parallel})$ in the infinite system. Fourier transforming (2.17) gives

$$G(\boldsymbol{r}^{\parallel}) = \int (2\pi)^{-2} \, \mathrm{d}^2\boldsymbol{q} |1 - \exp(\mathrm{i}\boldsymbol{q} \cdot \boldsymbol{r}^{\parallel})|^2 \cdot \langle |\boldsymbol{h}^{\perp}(\boldsymbol{q})|^2 \rangle. \tag{5.5}$$

The average phason strain $\mathbf{E}_0$ in (2.17) only involves the $\boldsymbol{q} = \mathbf{0}$ Fourier component and so it does not affect this result. (However, if $\mathbf{E}_0$ is sufficiently large, the higher powers in the expansion of $\sigma(\mathbf{E})$ become important and so the effective value of K can be changed).

† This also follows from equation (4.8), and the fact that grid lines have spacing $\frac{5}{2}$.

Also, Fourier transforming the 'free energy' given by (2.11) and (2.12) gives

$$\tilde{F} = \tfrac{1}{2} \int (2\pi)^{-2} \, \mathrm{d}^2 \boldsymbol{q} \, Kq^2 |\boldsymbol{h}^{\perp}(\boldsymbol{q})|^2 \tag{5.6}$$

and consequently

$$\langle |\boldsymbol{h}\perp(\boldsymbol{q})|^2 \rangle = d^{\perp}/Kq^2. \tag{5.7}$$

Substituting (5.7) into (5.5) and performing the integral gives

$$G(\boldsymbol{r}^{\parallel}) \simeq (d^{\perp}/\pi K) \ln(|\boldsymbol{r}^{\parallel}|/a) + \text{constant} \tag{5.8}$$

asymptotically, where a is the lattice cutoff (comparable to the tile edge length).

For the sixfold rhombus tiling, comparing equation (14) of Blöte and Hilhorst (1982) to equation (5.8) with $d^{\perp} = 1$ gives $K = \pi/9$. The only numerical results on correlation functions of this type for quasicrystal models are given by Elser (1987) for a decagon packing with tenfold symmetry—which, however, is a growth model rather than an equilibrium model. Elser's figure 7 shows the RMS fluctuations of $\boldsymbol{h}^{\perp}$ as a function of the sample dimension L; taking the square of the values plotted one can roughly fit $\langle |\boldsymbol{h}^{\perp}|^2 \rangle \approx 5 \ln L - 10$. If these fluctuations were controlled by a stiffness K, as in an equilibrium model, a calculation like that of (5.7), with $d^{\perp} = 2$, gives $\langle |\boldsymbol{h}^{\perp}|^2 \rangle \simeq (d^{\perp}/2\pi K) \ln(L/a) + \text{constant}$, which would correspond to $K \approx 0.06$ for Elser's data.

5.2.2. Longitudinal correlation function in strip. The most natural correlation function to consider would be the same as (2.17) but with strip boundary conditions, i.e. $G^{(\mathrm{W})}(0, L) \equiv \langle |\boldsymbol{h}^{\perp}(0, L) - \boldsymbol{h}^{\perp}(0, L) - \mathbf{E}_0(L, 0)|^2 \rangle$. However, a numerical calculation will have less trouble if we remove some short-distance corrections by using the mean 'height' over an entire layer:

$$\boldsymbol{h}^{\perp}_{\mathrm{av}}(L) = N_{\mathrm{W}}^{-1} \sum_{j=1}^{N_{\mathrm{W}}} \boldsymbol{h}^{\perp}(j, L) \tag{5.9}$$

(no ensemble averaging is done here). Essentially, this is the $q_x = 0$ component of the Fourier transform taken in the x direction but not the y direction. We define the longitudinal correlation function

$$G^{(\mathrm{W})}_{\mathrm{av}}(L) \equiv \langle |\boldsymbol{h}^{\perp}_{\mathrm{av}}(0) - \boldsymbol{h}^{\perp}_{\mathrm{av}}(L) - \mathbf{E}_0(L, 0)|^2 \rangle \tag{5.10}$$

subtracting an average phason strain as in (2.17). Paying attention to the correct normalisation of the Fourier transforms, we find

$$G^{(\mathrm{W})}_{\mathrm{av}}(L) = W^{-1} \int (2\pi)^{-1} \, \mathrm{d}q_{\mathrm{L}} |1 - \exp(\mathrm{i}q_{\mathrm{L}} L)|^2 / Kq_{\mathrm{L}}^2 = \tilde{D}L \tag{5.11}$$

where

$$\tilde{D} = d^{\perp}/2KW. \tag{5.12}$$

The result (5.12) means that $\boldsymbol{h}^{\perp}_{\mathrm{av}}(L)$ does a random walk, with a 'diffusion constant' $\tilde{D}$ inversely proportional to strip width. As we would expect from finite-size scaling ideas, (5.11) and (5.12) agree with (5.8) when L is of order W.

Equation (5.12) is essentially a relationship between the longitudinal correlation length in the finite strip geometry and the stiffness K. Such a relationship has independently been given in the context of the vector spin models by Fisher (1987) and also by Privman and Fisher (1987). It is analgous to the relationship of longitudinal correlation length and domain-wall free energy for Ising systems (Fisher 1969).

5.2.3. Transverse fluctuations within layer. Let

$$G^{(W)}_{\text{layer}} \equiv \langle |\boldsymbol{h}(0,0) - \boldsymbol{h}(W/2,0)|^2 \rangle. \tag{5.13}$$

This can be treated with the same manipulations as the first calculation, except that we can retain the finite sum over N_W. This gives the same dependence

$$G^{(W)}_{\text{layer}} = (d^\perp/2\pi K)\ln(W/a) + \text{constant} \tag{5.14}$$

except the finite sum gives a different constant term.

5.3. Correlation functions from transfer matrices

Our correlation functions depend on $\boldsymbol{h}^\perp$ which is *not* included in the state space of the transfer matrix as defined in § 5.1. That is, we know the probability to get from a starting-layer state to a given end-layer state, but not what change in $\boldsymbol{h}^\perp$ might occur between them. Formally, we can fix this by redefining the state space for layers by adjoining the value $\boldsymbol{h}^\perp_{\text{av}}$ from (5.9). (This is analogous to equation (18) of Luck (1983). Observe that the value of $\boldsymbol{h}^\perp$ at one site in a layer suffices to determine $\boldsymbol{h}^\perp$ for all other sites in the layer.)

Such a continuous (hence, infinite-dimensional) state space is difficult to handle by standard transfer-matrix techniques. However, $\boldsymbol{h}^\perp$ is just a slave variable in this iteration—it is affected by, but does not affect, the discrete part of the state space. This simplification permits us to express the desired correlations of $\boldsymbol{h}^\perp$ as traces of certain finite-dimensional matrices, and thereby do the calculation with a discrete state space after all.

There is one annoying difficulty in this procedure: all formulae derived from transfer matrices implicitly measure length in terms of the number of iterations N_L. As discussed at the end of § 5.1, this is not simply proportional to the length L. Hence a normalising factor L/N_L appears in the formulae below; for every strip and for every set of chemical potentials that might be applied in a numerical calculation, it is necessary also to measure this ratio.

5.3.1. Formula for K in terms of transfer matrix. Let $\mathbf{P}^L$ and $\mathbf{P}^R$ be the left and right eigenvectors corresponding to $\Lambda_{\max}$, the largest eigenvalue (for $\mathbf{T}$ is not in general symmetric), normalised so that their scalar product $(\mathbf{P}^L \cdot \mathbf{P}^R)$ is unity. Then the probability of layer μ occurring within the bulk is $P^L_\mu P^R_\mu$. We normalise the transfer matrix

$$\hat{\boldsymbol{T}} \equiv \Lambda^{-1}_{\max}\mathbf{T}$$

so that, e.g., $P^L_\nu \hat{T}_{\rho\nu}\hat{T}_{\nu\mu}P^R_\mu$ gives the probability of finding layers μ, ν and ρ in succession.

Also, let $\boldsymbol{u}_{\nu\mu}$ be the difference in $\boldsymbol{h}^\perp_{\text{av}}$ associated with going from old layer μ to new layer ν. We once again explicitly consider the possibility of non-zero phason strain in the longitudinal direction. The average phason tilt is

$$\mathrm{d}\langle \boldsymbol{h}^\perp_{\text{av}}(L)\rangle/\mathrm{d}L = (N_L/L)\langle \boldsymbol{u}\rangle$$

where

$$\langle \boldsymbol{u}\rangle \equiv \sum_{\mu\nu} P^L_\nu T_{\nu\mu} P^R_\mu \boldsymbol{u}_{\nu\mu}. \tag{5.15}$$

It is convenient to define matrices $\mathbf{U}^{(m)}$ (for $m = 1, \ldots, d^\perp$) with elements

$$U^{(m)}_{\beta\alpha} \equiv u^{(m)}_{\beta\alpha}\hat{T}_{\beta\alpha} \tag{5.16}$$

so that, with matrix multiplication contracting the Greek indices,

$$\langle \boldsymbol{u} \rangle = (\mathbf{P}^{\mathrm{L}}, \mathbf{U}\mathbf{P}^{\mathrm{R}}). \tag{5.17}$$

The variance of $\boldsymbol{h}_{\mathrm{av}}^{\perp}$ is more complicated. We want to calculate

$$\tilde{D} \equiv (N_{\mathrm{L}}/L)\, \mathrm{d}(\langle |\boldsymbol{h}_{\mathrm{av}}^{\perp}(L)|^2 \rangle - |\langle \boldsymbol{h}_{\mathrm{av}}^{\perp}(L) \rangle|^2)/\mathrm{d}N_L \tag{5.18}$$

which by (5.12) equals $d^{+}/2KW$. Let

$$\boldsymbol{v}_{\nu\mu} \equiv \boldsymbol{u}_{\mu\nu} - \langle \boldsymbol{u} \rangle \tag{5.19}$$

and define matrices $\mathbf{V}^{(m)}$ analogously to (5.16); obviously

$$\langle \boldsymbol{v} \rangle = (\mathbf{P}^{\mathrm{L}}, \mathbf{V}\mathbf{P}^{\mathrm{R}}) = \mathbf{0}. \tag{5.20}$$

The part of (5.18) due to the fluctuation of $\boldsymbol{u}$ values in one layer can be expressed in terms of $\mathbf{V}_{(2)}$ with elements

$$V_{(2),\beta\alpha} \equiv |\boldsymbol{v}_{\beta\alpha}|^2 T_{\beta\alpha}. \tag{5.21}$$

However, the $\boldsymbol{v}$ are correlated between successive layers. The correlations decay geometrically as powers of $\hat{\mathbf{T}}$ and summing this geometric series one can derive

$$\tilde{D} = \frac{N_{\mathrm{L}}}{L}\left((\mathbf{P}^{\mathrm{L}}, \mathbf{V}_{(2)}\mathbf{P}^{\mathrm{R}}) + 2 \sum_{m=1}^{d^{-}} (\mathbf{P}^{\mathrm{L}}, \mathbf{V}^{(m)}(\mathbf{1}-\hat{\mathbf{T}})^{-1}\mathbf{V}^{(m)}\mathbf{P}^{\mathrm{R}}) \right). \tag{5.22}$$

To be precise, (5.22) should have the pseudo-inverse of $(\mathbf{1}-\hat{\mathbf{T}})$ since this matrix is singular. But (5.22) is still well defined: the singular matrix is surrounded by $\mathbf{V}^{(m)}$ factors on both sides which (by (5.20)) annihilate the singular subspace $\mathbf{P}^{\mathrm{R}}\mathbf{P}^{\mathrm{L}}$.

5.3.2. Monte Carlo transfer-matrix method. An alternative method which is well adapted to the random-tiling problem is the Monte Carlo transfer-matrix (MCTM) method (Nightingale and Blöte 1986).

Repeated multiplication of an initial distribution vector $\mathbf{P}_{\mathrm{I}}$ by the transfer matrix gives a vector $(\mathbf{T}^{N_{\mathrm{L}}}\mathbf{P}_{\mathrm{I}})_{\nu}$, which is calculated by brute force in the ordinary iterative approach. The MCTM approach represents this vector by a discrete collection of M layer states $\{\nu\}$. Since we do not know $\Lambda_{\max}$ beforehand, we must approximate $\hat{\mathbf{T}}$ by $\tilde{\mathbf{T}} \equiv \Lambda_{\mathrm{est}}^{-1}\mathbf{T}$ where Λ_{est} is a running estimate of $\Lambda_{\max}$. In every iteration we proceed as follows.

(i) For each ν represented in our list, we calculate the total weight of possible new states, $w_{\nu} \equiv \Sigma_{\rho}\, \tilde{T}_{\rho\nu}$. We choose an integer $M_{\nu} \geqslant 0$ by a random process that satisfies $\langle M_{\nu} \rangle = w_{\nu}$, and then if necessary replicate or remove ν so that M_{ν} copies remain.

(ii) For each state ν in the modified list, we pick at random one of the next states with the weight $\tilde{T}_{\rho\nu}/w_{\nu}$.

Each state in the list, with its precursors in previous iterations, defines a tiling configuration. In fact, the MCTM method generates a sample of configurations with the correct statistical weight. Thus, we can directly evaluate any desired correlation function, without needing to calculate additional eigenvalues or sums such as (5.22).

The general advantages of the Monte Carlo transfer-matrix method are as follows.

(i) It needs less computation. Say each step in a layer state has μ choices ($\mu = 4$ for the tenfold tiling). The standard method requires storing, calculating and multiplying the entire $\mu^{N_{\mathrm{w}}} \times \mu^{N_{\mathrm{w}}}$ transfer matrix ($\mathrm{O}(\mu^{2N_{\mathrm{w}}})$ operations). With the MCTM

approach, this is done only for the M states in the list so the work per iteration is at most $O(\mu^{N_W}M)$ which permits wider strips. In fact, for the random-tiling models the problem of calculating $T_{\nu\mu}$ factors into independent intervals (see § 4.3), so the work is only $O(N_W M)$ in this case!

(ii) It handles systems with infinite-dimensional state spaces, such as arise from continuous degrees of freedom (in particular, $\boldsymbol{h}^\perp$ for the tilings).

The MCTM's disadvantage, of course, is its statistical errors which go as $M^{-1/2}$.

5.4. Ways to extract K from transfer-matrix data

It is instructive to review the analogous question for the $d = 2$ Ising model, at sufficiently low T that the correlation length exceeds the strip width W. The principal difference is that the Ising model has a *discrete* up-down symmetry whereas the random tilings have a *continuous* symmetry under displacements of $\boldsymbol{h}^\perp$. Corresponding to these symmetries are the excitations which give disorder: domain walls in Ising models and long-wavelength phason fluctuations in the tilings. The respective 'stiffnesses' of the excitations are the domain-wall free energy σ and the phason stiffness K.

In seeking the value of the stiffness, for both the Ising and the tiling cases, there are in principle 2×2 ways, since (i) we can use excitations either *longitudinal* to the strip or *transverse* to it; the transverse ones are simpler to express in terms of transfer matrices since they are simultaneous in 'iteration time', and (ii) we can probe the excitations, either by *forcing* them and measuring the change in the free energy, or by looking at *fluctuations* in equilibrium; note that domain walls have a higher energy cost than long-wavelength phasons, so fluctuations are easier to see in continuous models (such as the tiling with $\boldsymbol{h}^\perp$) than in Ising models.

5.4.1. Forcing a transverse excitation. In general, this is the simplest to implement and often the most reliable. (See Luck (1981) for an example in a roughening context.) For Ising models, this is done by applying antiperiodic boundary conditions so as to force one domain wall to run the entire length of the strip. For the tenfold-tiling model, this can be done by choosing the numbers of L^+, L^-, S^+, and S^- in a layer so as to impose a given phason strain in the x direction. (In fact, we cannot avoid this—the ideal irrational number ratio τ (see equations (4.5)) is impossible with a finite strip width.)

5.4.2. Forcing a longitudinal excitation. For tiling models, we can couple to the phason strain by adding chemical potentials (energy terms) weighting different orientations of tiles differently, as in (2.13). Evaluating the phason strain would require evaluating $\mathrm{d}(\boldsymbol{h}^\perp_{\mathrm{av}}(L))/\mathrm{d}L$ by (5.15) or using the MCTM method. (The Ising analogue would be to add a slowly modulated field $H(L)$, which is awkward.)

5.4.3. Transverse fluctuations. This is practicable only for tiling models. We need merely evaluate (5.13).

5.4.4. Longitudinal fluctuations. A more traditional approach would involve labelling the eigenvectors according to a wavevector $\boldsymbol{q}^\perp$ which describes their transformation under translations in $\boldsymbol{h}^\perp$, and then considering the $\boldsymbol{q}^\perp$ dependence of the largest

eigenvalue of each subspace. This is the spirit of the analysis of Luck *et al* (1983) for a pinning model; it leads (Henley unpublished) to the analogue of the Fisher relation between σ and the eigenvalues for the Ising case (Fisher 1969). Here, the more streamlined approach appears to be to find $\tilde{D}$ (5.18) directly, either from (5.22) or by using the MCTM technique.

5.5. Results for very narrow strips

For some strips with $N_W = 3$ and $N_W = 4$ the transfer matrix (5.1) was constructed by hand, and the largest eigenvalue and corresponding eigenvalue were determined. To reduce the size of the matrices, I used the symmetries of cyclic permutation of the strings representing the layers, and also reflection around the x axis if $N(L^+) = N(L^-)$, $N(S^+) = N(S^-)$. The entropies quoted are for the fixed-N_L ensemble, which should be slightly different numerically from the true value as noted at the end of § 5.1.

For $N_W = 3$, for layers containing $L^+ + L^- + S^+$, there are only two states modulo the symmetry. Then $\Lambda_0 = (5+\sqrt{13})/2$. There are 1.639 fat rhombi per layer and exactly the same number of thin rhombi, so the area per layer is $A = 2.6514\bar{A}$. Hence we get an entropy $S_0 = \ln \Lambda_0 / A \simeq 0.470\bar{A}^{-1}$, and a ratio $n_{\text{fat}}/n_{\text{thin}} = 1$.

For $N_W = 4$, for layers containing $L^+ + L^- + S^+ + S^-$, there are five states modulo symmetry. We get $\Lambda_0 \simeq 7.547$, 1.969 fat and 0.963 thin rhombi per layer, $S_0 \simeq 0.673\bar{A}^{-1}$, and $n_{\text{fat}}/n_{\text{thin}} \simeq 2.045$.

These numbers seem consistent with $S_0 \simeq 0.5\bar{A}^{-1}$, but manifestly larger strips are needed just to get an approximation. (Note that $N_W = 4$ is the smallest strip for which all three rules of § 4.3 apply.) To get reliable results for the random tiling with tenfold symmetry, the strip should not only be wide but have a good approximant to the ratio $N(L^\pm)/N(S^\pm) = \tau$. The first strips of this type are $N_W = 6$, with $2L^+ + 2L^- + S^+ + S^-$ making 15 states, and $N_W = 10$, with $3L^+ + 3L^+ + 2S^+ + 2S^+$ making 1260 states.

6. Discussion: summary, applications and generalisations

Random tilings provide a minimal model for a particular type of random quasicrystal packing. This can usefully be represented as a hypersurface in a higher-dimensional space (§ 2), and questions of long-range order can be translated into questions about the orientation dependence of the 'surface free energy' and roughness of the hypersurface. I have displayed formulae explicitly relating its orientation (i.e. the 'phason strain') to the frequencies of tiles, which are useful if (as in § 5) we wish to bias for a particular strain.

In §§ 3 and 4, I have presented schemes to decompose tilings into layers, using a modest number of degrees of freedom per step in the layer, and properly representing each distinct tiling by a different configuration.

Among other things, these decompositions are labelling schemes—ways to map the quasicrystal sites to a lattice†. Such decompositions can be used for transfer matrices defined on a fixed given (say ordered) Penrose tiling geometry, to test other approaches for several problems: ferromagnetic Ising spins on tiling sites, both bulk critical

† The impossibility of constructing labelling schemes with additional desirable properties has been discussed by Frenkel *et al* (1986).

properties (e.g. Godrèche *et al* 1986) and interface roughening (Henley and Lipowsky 1987, Garg and Levine 1987, Ho *et al* 1987) or transmission matrices to study electronic states on tilings (e.g. Kohmoto and Sutherland 1986).

Following from the decomposition rules were relatively simple short-range transition rules specifying which configurations are allowed and enabling the construction of transfer matrices. The only remaining defect is that, to calculate the entropy at fixed area, one must repeat the calculation at various pressures and do a Legendre transformation.

The approach works especially well with the Monte Carlo transfer method approach (§ 5.3). The branching process of the Monte Carlo transfer-matrix method ensures a correctly weighted ensemble because layers which lead to more statistical weight in subsequent layers can have more 'descendents.' However, if we omit the step in which we replicate or remove states, it gives a growth model which does not look ahead. It has been found that growth induces phason strain in an aggregation model; it would be interesting to verify similar effects in a tiling model.

Similar decomposition and transition rules have been devised for two other important two-dimensional tilings (Henley unpublished). One of these, with tenfold symmetry, can be thought of as a tiling by isosceles triangles: acute, with sides $(1, \tau, \tau)$ and obtuse, with sides $(\tau, 1, 1)$. The vertices are both (i) the sites of large 'atoms' in the model of Widom *et al* (1987) and Lançon *et al* (1986) and (ii) the sites of decagons in the model of Elser (1987), for a set of well ordered configurations.

The other tiling, with 12-fold symmetry, is the triangle-square tiling; this is much simpler than the tenfold rhombus tiling, because there are only four vertex types instead of 53. The decomposition into layers uses a strip oriented 15° away from tile edge directions and three states for each step: $A^{\pm}$ along the tile edges, analogous to $L^{\pm}$ in § 4, and 0 in the transverse direction along a square diagonal, somewhat analogous to $S^{+}S^{-}$. Analogous to the formulations in §§ 3 and 4, the numbers of $A^{\pm}$ and 0 steps are conserved from layer to layer.

It is illuminating to compare this transfer-matrix formulation to that used by Kawamura (1983) and mentioned in § 1.2. Kawamura divided into layers in a similar fashion, using, however, eight states per step, and each tiling can be transcribed uniquely. However, the strings of states do *not* correspond one-to-one with possible layer configuration: many such strings correspond to impossible layers so the number of states is much less than 8^{N_W}. For the allowed ones, the transfer matrix breaks up into disconnected subspaces. (The physical significance is clearer in my formulation—these just correspond to the different (conserved) numbers of $A^{\pm}$ and 0 steps.) The number of states in the largest subspace is 95, 299, 885 and 2623, for $N_W = 3$, 4, 5 and 6 respectively, which is numerically well fitted by 3.6×3^{N_W}. This is not surprising, since (in my formulation) the total number of layer states in *all* subspaces is manifestly 3^{N_W}. (Kawamura's prefactor is larger since his layer states also depend on the configuration of steps in the next layer.) The transition rules of Kawamura's formulation have the advantage of being local, like a spin model (whereas my rules sometimes allow interchanges of steps across large distances). However, they are difficult to grasp, since they consist of a list of all the 107 cases allowed out of the 8^4 conceivable combinations of four neighbouring states.

Finally, in § 5, I have discussed possible methods for extracting the parameters from transfer matrices. In fact (§5.4), all four conceivable methods seem useable (which is not true for Ising models). The redundant information from using more than one method, and from considering phason strains in different directions relative

to the strip axis, will be important for confirming whether Elser's conjecture of the form (2.12) is correct.

In three-dimensional tilings with icosahedral symmetry, a transfer-matrix approach is also possible, of course. However, in contrast to the 2D case, neither the decomposition rules nor the transition rules will be simple.

Acknowledgments

For helpful ideas and comments, I wish to thank L C Chen, M E Fisher, T L Ho, H Kawamura, T C Lubensky, M P Nightingale, F Spaepen and M Widom. I especially thank Veit Elser, whose concepts were used throughout, and Larry Shaw for his detailed comments on the manuscript. This work was supported by NSF grant DMR-8451921 and an IBM Postdoctoral Fellowship.

Note added. Very recently, Shaw (1987) has implemented the Monte Carlo transfer-matrix method for the sixfold symmetric tiling described in § 3, verifying the known exact values of the entropy per tile S_0 (quoted above, after equation (3.3)) and stiffness K (quoted above, after equation (5.8)). (The latter is extracted by the method of forcing a transverse phason strain.) Also, the behaviour of interfaces in tilings, studied by Garg and Levine (1987), Henley and Lipowsky (1987) and Ho *et al* (1987), has been generalised to the random tilings discussed in this paper by Lipowsky and Henley (1988).

Note added in proof. Equation (2.12), and the sentence following, are false. Even if the complementary space has only one irreducible component it is still common that there is more than one phason stiffness constant. That is, the complementary space *vectors* are one irreducible representation of the p-fold symmetry group, but the physical complementary space *tensor* **E** is a reducible representation (Bak 1985). For tenfold symmetry, the correct form is

$$\tfrac{1}{4}K_1[(E_{11}+E_{22})^2+(E_{12}-E_{21})^2]+\tfrac{1}{4}K_2[(E_{11}-E_{22})^2+(E_{12}+E_{21})^2+\tfrac{1}{2}K_3[E_{31}^2+E_{32}^2]$$

in place of (4.2). All formulae involving K in § 5 should be modified accordingly, but the qualitative conclusions there and in § 2.6 are unchanged.

References

Bak P 1985 *Phys. Rev.* B **32** 5764
Bancel P A, Heiney P A, Stephens P W, Goldman A I and Horn P M 1985 *Phys. Rev. Lett.* **54** 2422
Blöte H W J and Hilhorst H J 1982 *J. Phys. A: Math. Gen.* **15** L631
Chen L C and Spaepen F 1988 *Materials Science and Engineering 89* to be published
de Bruijn N G 1981 *Proc. Konink. Ned. Akad. Wetensch.* A **84** 39, 53
Elser V 1984 *J. Phys. A: Math. Gen.* **17** 1509
—— 1985a *Phys. Rev. Lett.* **54** 1730
—— 1985b *Phys. Rev.* B **32** 4892
—— 1987 *Proc. 15th Int. Colloq. on Group Theoretical Methods in Physics* vol 1, ed R Gilmore (Singapore: World Scientific) p 162
—— 1988 *NATO Advanced Research Workshop on New Theoretical Concepts in Physical Chemistry* ed A Amann, L S Lederbaum and W Gans (Dordrecht: D Reidel) to be published
Elser V and Henley C L 1985 *Phys. Rev. Lett.* **55** 2883
Fisher M E 1969 *J. Phys. Soc. Japan Suppl.* **26** 87
—— 1985 *J. Appl. Phys.* **57** 3265
Frenkel D, Henley C L and Sigggia E D 1986 *Phys. Rev.* B **34** 3649
Gähler F 1986 *J. Physique Colloq.* **47-C3** 115
Garg A and Levine D 1987 *Phys. Rev. Lett.* **59** 1683
Godrèche C, Luck J M and Orland H 1986 *J. Stat. Phys.* **45** 777

Guyot P and Audier M 1985 *Phil. Mag.* B **52** L15
Heiney P A, Bancel P A, Horn P M, Jordan J L, La Placa S, Angilello J and Gayle F W 1987 *Science* **238** 660
Henley C L 1987 *Comment. Cond. Mat. Phys.* **13** 59
—— 1988 *Phys. Rev.* B to be submitted
Henley C L and Elser V 1986 *Phil. Mag.* B **53** L59
Henley C L and Lipowsky R 1987 *Phys. Rev. Lett.* **59** 1679
Ho T L, Jaszczak J A, Li Y H and Saam W F 1987 *Phys. Rev. Lett.* **59** 1116
Horn P M, Malzfeldt W, DiVincenzo D P, Toner J and Cambino R 1986 *Phys. Rev. Lett.* **57** 1444
Kantor Y, Kardar M and Nelson D R 1986 *Phys. Rev. Lett.* **57** 791
Kasteleyn P W 1963 *J. Math. Phys.* **4** 287
Katz A and Duneau M 1986 *J. Physique* **47** 181
Kawamura H 1983 *Prog. Theor. Phys.* **70** 352
Kohmoto M and Sutherland B 1986 *Phys. Rev. Lett.* **56** 2740
Lançon F, Billard L and Chaudhari P 1986 *Europhys. Lett.* **2** 625
Leung P W, Henley C L and Chester G V 1987 unpublished
Levine D and Steinhardt P J 1984 *Phys. Rev. Lett.* **53** 2477
Lipowsky R L and Henley C L 1988 unpublished
Lubensky T C, Ramaswamy S and Toner J 1985 *Phys Rev* B **32** 7444
Lubensky T C, Socolar J E S, Steinhardt P J, Bancel P A and Heiney P A 1986 *Phys. Rev. Lett.* **57** 1440
Luck J M 1981 *J. Physique Lett.* **42** L275
—— 1982 *J. Phys. A: Math. Gen.* **15** L169
Luck J M, Leibler S and Derrida B 1983 *J. Physique* **44** 1135
Minchau B, Szeto K Y and Villain J 1987 *Phys. Rev. Lett.* **58** 1960
Nightingale M P and Blöte H W J 1986 *Phys. Rev.* B **33** 659
Orrick W P 1987 *Senior thesis* Princeton University
Privman V and Fisher M E 1985 *J. Appl. Phys.* **57** 3327
Rottman C and Wortis M 1984 *Phys. Rep.* **103** 59
Shaw L 1987 private communication
Shechtman D, Blech I, Gratias D and Cahn J W 1984 *Phys. Rev. Lett.* **53** 1951
Socolar J E S, Lubensky T C and Steinhardt P J 1986 *Phys. Rev.* B **34** 3345
Socolar J E S, Steinhardt P J and Levine D 1985 *Phys. Rev.* B **32** 5547
Spaepen F 1976 *Scr. Metall.* **10** 257
Stephens P W and Goldman A I 1986 *Phys. Rev. Lett.* **56** 1168
Wang N, Chen H and Kuo K H 1987 *Phys. Rev. Lett.* **59** 1010
Wannier G H 1950 *Phys. Rev.* **79** 357
Widom M, Strandburg K J and Swendsen R H 1987 *Phys. Rev. Lett.* **58** 706
Wilkinson J H 1965 *The Algebraic Eigenvalue Problem* (Oxford: Oxford University Press)